COMPUTER-ASSISTED SKIN LESION DIAGNOSIS AND MELANOMA CANCER DETECTION

A DISSERTATION

SUBMITTED IN PARTIAL FULFILLMENT OF THE REQUIREMENTS

FOR THE AWARD OF THE DEGREE

OF

MASTER OF TECHNOLOGY

IN

Signal Processing and Digital Design

Submitted by

Sunny thakur

(2K19/SPD/19)

Under the supervision of

Prof. INDU SREEDEVI (Prof, ECE Dept.)

DEPARTMENT OF ELECTRONICS AND COMMUNICATION

DELHI TECHNOLOGICAL UNIVERSITY

(Formerly Delhi College of Engineering)

Bawana Road, Delhi -110042

JUNE 2021

CONTENTS

PLAGIARISM REPORT

DEPARTMENT OF ELECTRONICS AND COMMUNICATION ENGINEERING
DELHI TECHNOLOGICAL UNIVERSITY
(Formerly Delhi College of Engineering)
Bawana Road, Delhi-110042

CANDIDATE'S DECLARATION

I, **Sunny Thakur,** student of M.Tech (Signal Processing and Digital Design), hereby declare that the project Dissertation titled **"COMPUTER-ASSISTED SKIN LESION DIAGNOSIS AND MELANOMA CANCER DETECTION"** which is submitted by me to the Department of Electronics and Communication Engineering, Delhi Technological University, Delhi in partial fulfillment of the requirement for the award of the degree of Master of Technology is original and not copied from any source without proper citation. This work has not previously formed the basis for the award of any Degree, Diploma Associateship, Fellowship, or other similar title or recognition.

Place: Delhi **Sunny Thakur**
Date: 23rd July 2021

DEPARTMENT OF ELECTRONICS AND COMMUNICATION ENGINEERING
DELHI TECHNOLOGICAL UNIVERSITY
(Formerly Delhi College of Engineering)
Bawana Road, Delhi-110042

CERTIFICATE

I hereby certify that the Project Report titled "**COMPUTER-ASSISTED SKIN LESION DIAGNOSIS AND MELANOMA CANCER DETECTION**" which is submitted by **Sunny Thakur**, **2K19/SPD/19** of Electronics and Communication Department, Delhi Technological University, Delhi, in partial fulfillment of the requirement for the award of the degree of Master of Technology, is a record of the project work carried out by the students under my supervision. To the best of my knowledge, this work has not been submitted in part or full for any Degree or Diploma to this University or elsewhere.

Place: Delhi
Date: 23rd July 2021

Prof. S. Indu
SUPERVISOR

ACKNOWLEDGEMENT

I would like to express my deep gratitude and indebtedness to my supervisor Prof. S. Indu for encouragement and guidance. Her invaluable meticulous and critical supervision in every phase of this work inspired me in innumerable ways.

I also express my gratitude to Dr. N. S. Raghava, HOD, Department of Electronics and Communication Engineering, who encouraged me in many ways and provided all the help that he could as the head of the Department for the smooth completion of my research work.

Special acknowledgments are due to all the faculty members of the ECE Departments and other supporting staff for helping during my M. Tech course.

Finally, I wish to express my sincere gratitude to my family members for their patience and sacrifice throughout the work. This thesis is dedicated to them as a token of my gratitude and love.

Sunny Thakur

ABSTRACT

Skin cancer is among the most common cancer types that affect people across the world. According to the American Cancer Society statistical data, an approximate increase of new melanoma cases will be 5.8%, and the death rate will increase by 4.8%. Medical specialists believe that early diagnosis is the key to effective treatment. The preliminary visual examination of skin lesions by dermatologists had a low accuracy rate (60-70%). However, melanoma-type cancer is hard to distinguish from nevus. Machine learning and CNN applications on dermatoscopic images for the early detection of melanoma cancer produced tremendous outcomes in the past few decades. The primary objective of this thesis is to develop a robust CAD system for the analysis of skin lesion images. At the same time, the secondary objective is to study the methodologies adopted in many research articles on skin cancer identification and classification. In this thesis, we proposed a modified capsule UNET architecture for segmentation tasks and FixEfficientNet as a classification model and performed analysis on ISIC 2017 and PH2 datasets.

Moreover, we present a brief discussion of recent approaches evolved to detect and classify skin cancer and perform a comparative analysis of performances achieved by different systems developed for skin cancer detection and classification. The proposed work achieved an 88.3% dice score, 93.4% accuracy, 94.7 % sensitivity, and 96.3% of specificity. Even though these approaches achieved a significant result, there are many challenges for successful diagnostics. We also discussed these challenges and proposed potential advancement as future work to overcome these challenges. The comprehensive analysis of different methods suggests that advanced deep learning algorithms provide a robust technique for the multi-class classification of pigmented skin lesion images.

LIST OF FIGURES

LIST OF TABLES

ABBREVIATIONS

Abbreviation	Full-Form
BCC	Basal cell carcinoma
SCC	Squamous Cell Carcinoma
MRI	Magnetic Resonance Imaging
CM	Confocal microscopy
OCT	Optical Coherence Tomography
CAD	Computer-Aided Diagnosis
CMYK	Cyan Magenta Yellow Black
DOG	Derivative of Gausian
HOG	Histogram of Oriented Gradients
BFF	Best First strategy for Feature selection
MDLM	Minimum Description Length Method
LVF	Las Vegas Filter
SFS	Sequential forward selection
SBS	Sequential Backward selection
POSS	Proportional overlapping score
BDS	Bidirectional search
ANN	Artificial Neural Network
ELM	Extreme learning Machine
AUC	Area Under Curve
CNN	Convolutional Neural network
RBF	Radial Basis Function
FC	Fully Connected Layer
FrCN	Full resolution Convolutional network
GAN	Generative Adviseral Network
UNet-SCDC	skip connection and diluted convolution UNet
MSCN	Multi-Scale Convolutional network
DDN	Dense Deconvolutional Network
LeNet	Lecun's Network
VGG	Visual Geometry Group
GLCM	Gray-Level Co-Occurrence Matrix
SURF	Speeded-Up Robust Features
LBP	Local Binary Patterns
RPN	Region Proposal Network
DPN	Dual-Path Network
DCNN	Deep Convolutional Neural Network
ResNet	Residual Network
DenseNet	Densely Connected Network
FC	Fully Connected

LRN	Local Response Normalization
ReLU	Rectified Linear Unit
MACs	Multiply-Accumulate
ELM	Ensemble Learning Model
PSO	Particle Swarm Optimization
LDA	Linear Discriminant Analysis

CHAPTER-1

INTRODUCTION

1.1 BACKGROUND

Skin cancer is among the most common cancer types across the world. It has a severe impact on countries that have sunny climate conditions, such as America and Europe. In the past decade, invasive melanoma cancer cases increase by 44% annually reported by the American cancer society, 2021 [1]. In America, more than two patients lost their life due to skin cancer every hour. The Incidence and mortality rate of melanoma and non melanoma cancer across world is shown in fig1 and fig 2 respectively. It was clearly observed that the new incidence of melanoma cancer cases are more in European and American while the number of deaths are more in Asian countries as compared to European countries. This trends suggests that the skin cancer in Asian countries are generally diagnosed in later stages as the ratio of new cancer diagnosed and death is small. The other important observation that can be deduced from the statistics is that the number of cases for non melanoma cancer are more than melanoma and it was diagnosed and treated successfully as the number of deaths was relatively lower than melanoma cancer.

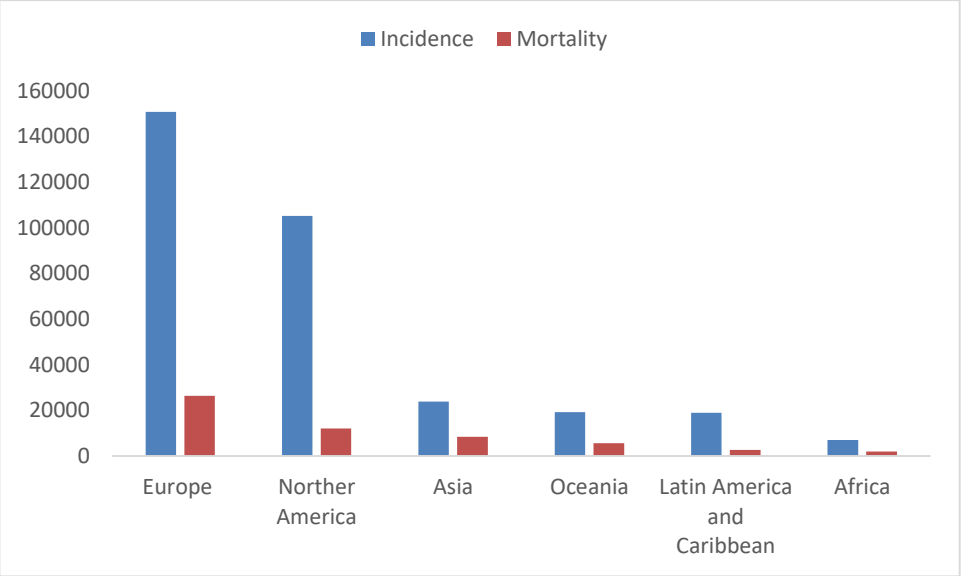

Fig. 1 Worldwide statistics for Melanoma Skin cancer
Source: GLOBOCAN 2020

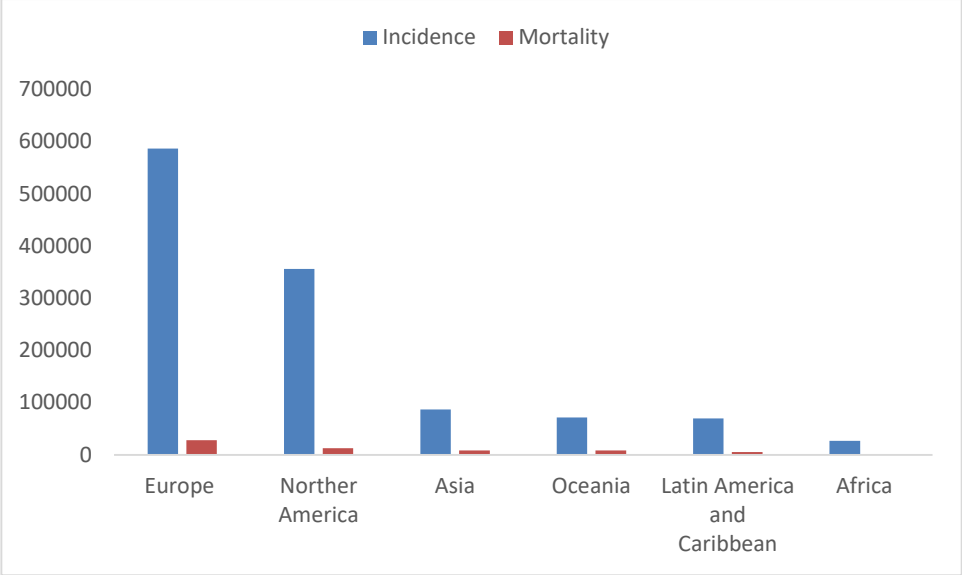

Fig. 2 Worldwide statistics for Non Melanoma skin cancer
Source: GLOBOCAN 2020

Skin cancer based on the depth of skin damage can be classified into two types non-melanoma and melanoma cancer. Non-melanoma cancers include Basal cell carcinoma (BCC) and squamous cell carcinoma (SCC). Non-melanoma cancers are generally treated successfully by the dermatologist. Melanoma cases are challenging to diagnose, and even trained experts cannot distinguish between common nevus and melanoma skin lesions. The majority of deaths occur due to melanoma skin cancer. The mortality rate across different countries illustrated in fig.3 indicates that deaths in European countries account for 46% of total deaths. However, the five-year survival rate for melanoma is 92 % if diagnosed early. Diagnosing melanoma at later stages significantly reduces the survival rate. Hence the early diagnosis of skin cancer will help patients to cure fast without further implications.

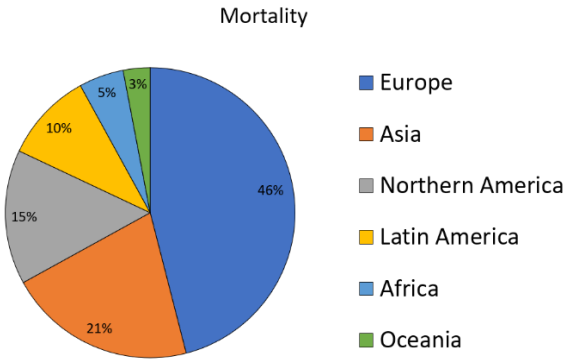

Fig. 3 Mortality rate of melanoma in different parts of the world

Conventional clinical methods for the diagnosis of skin lesions include visual inspection and biopsy by a dermatologist. These approaches require high expertise to study the growth and distinguish among the melanoma, dysplastic nevus, and common nevus. Moreover, the experts reached 90% sensitivity and 59 % specificity in skin cancer's successful diagnosis[2]. Thus, the need for a computer-aided diagnostics (CAD) system arises. CAD systems decrease mortality and provide an efficient platform to study aspects of skin cancer.

Over the past decade, many CAD systems have been proposed to identify skin cancer, specifically melanoma cancer, and study its malignancy extent. Most CAD systems involve the study of clinical images acquired using dermoscopy[3]. The pigmented skin lesions were first segmented and then applied many feature engineering methods to extract structural features. Finally, the classification algorithm classified the pigmented skin lesion among melanocytic nevi, benign keratosis, melanoma, BCC, actinic keratoses, dermatofibroma, and vascular lesions. The famous classification algorithm includes Bayes classifier, K-NN, Decision tree (DT), and support vector machine (SVM). Moreover, some ensemble learning techniques such as XGBoost and AdaBoost also achieved significant classification results.

Recently, Convolutional Neural Network (CNN) and Deep learning(DL) methods have been widely used to segment and classify medical images. UNet and encoder-decoder networks have become very popular segmentation techniques and achieve promising results. The famous deep learning algorithm used for classifying pigmented skin lesion images includes InceptionNet v3, ResNet, and DenseNet. Although these methods involve automatic feature extraction, these methods did not achieve more than 90% accuracy. Eddine et al.[4] proposes an ensemble technique which combines three best CNN model and achieves outstanding results. Some research works on hybrid CNN approaches, which utilizes CNN as a feature extractor and predictive classifier such as KNN and SVM for classification. These methods achieved promising results.

1.2 THESIS OVERVIEW

This documentation includes complete studies and implementation details. All the work is inscribed step by step in chapters as given below:

- Chapter 2 provide the brief description of skin anatomy and skin lesions classification. The different types of skin cancer is also discussed in this chapter.
- Chapter 3 includes the overview of computer aided diagnostics system. This chapter will provide fundamental knowledge which sets the stage for later work. It includes a brief study of handcraft-based CAD systems and CNN-based approaches. Moreover, an illustration of the different image acquisition processes, feature selection methods, and a summary of different proposed CNN architectures with their performances are provided.
- Chapter 4 contains implementation details. This chapter includes step-by-step skin lesion analysis and melanoma detection using dermoscopic images of skin lesions.
- Chapter 5 describes the result and analysis of the proposed methodology that we have done to complete experimental work.
- Finally, the thesis is concluded in chapter 6. This chapter describes the challenges faced during the completion of this work and suggests some future work that researchers can do to improve the results of the proposed network.

CHAPTER-2

SKIN ANATOMY AND CANCER TYPES

2.1 SKIN ANATOMY

Skin is the largest organ of human body as it covers all body parts. It has three layers Epidermis, Dermis and Subcutaneous fat layer. Epidermis is the topmost and thin layer of skin contains three type of cells Squamous cell, basal cell and melanocytes. Squamous cell are flat and peel off the skin surface as new cell forms. Basal cells are the cell found in inner part and generally divides to form new cells which moves upwards and replace squamous cells. The most important cell of epidermis is melanocytes which make brown pigmentation of skin. It serve as protective layer for inner part of skin from harmful UV rays of sun. The uncontrolled growth of squamous cells and basal cells leads to squamous cell carcinoma and basal cell carcinoma. Whereas, the abnormal growth of melanocytes leads to rare but dangerous skin cancer called melanoma cancer. The dermis constitutes the middle section of skin and contains blood vessels, lymph vessels, hair follicles and collagen bundles. It is responsible for sensory touch and flexibility of skin. The deepest layer of skin contains collagen fibres and fat cells. It is responsible for shock absorption and regulates temperature of body. Figure 4 shows the anatomy of skin.

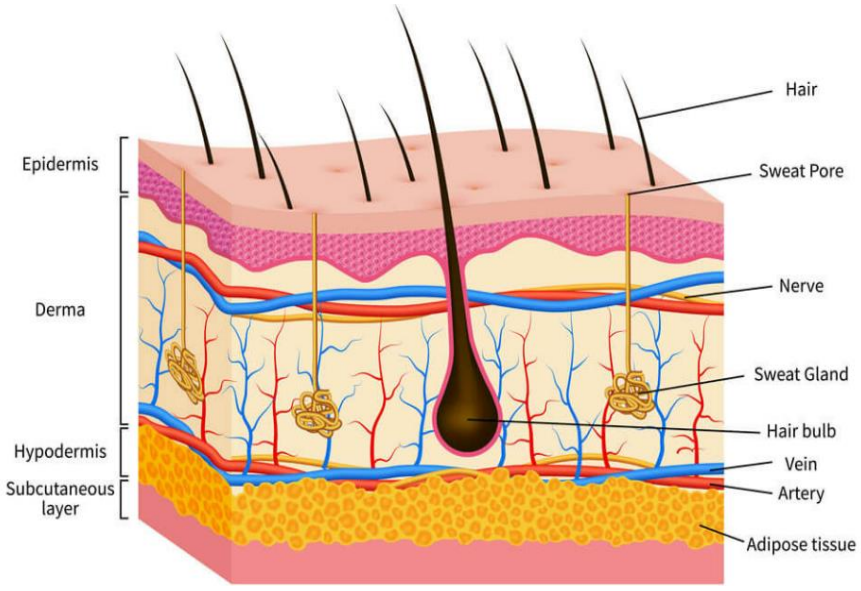

Fig. 4 Skin anatomy

2.2 SKIN LESION

Skin lesions are defined as the area of skin having different characterstics from the surrounding skin. It includes bumps, coloured patches, cysts and blisters. It generally appears to those part of skin which are exposed to sun regularly. In many cases the skin lesions diagnosed are not benign and can be easily treated by dermatologists. But in some cases, the skin lesions cause deaths if not diagnosed early. They are classified into two groups melanocytic and non-melanocytic skin lesions.

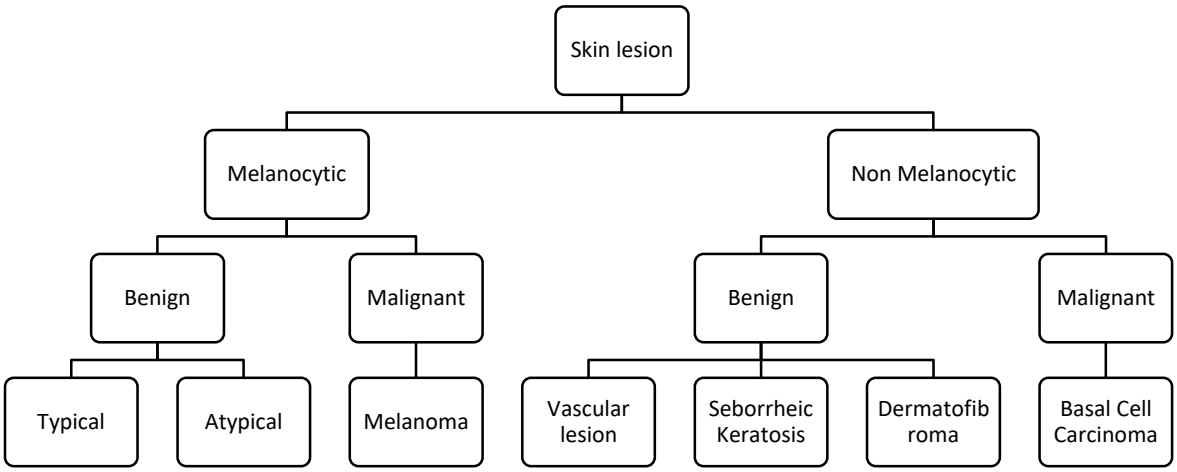

Fig. 5 Skin lesion classification hierarchy

Melanocytic skin lesions are originated from melanocytes cells. If the DNA of these cells are not altered they are called benign whereas, if DNA alteration present then these cells proliferated into lymph system and metastatize to damage other organs, and comes into malignant or melanoma category. Skin lesion originated from other cells of epidemis are classified under non melanocytic category. Non melanocytic skin lesions incorporate benign skin lesion such as vascular lesion, seborrheic keratosis and dermatofibroma and basal cell carcinoma as malignant type.

2.3 SKIN CANCER TYPES

2.3.1 Non Melanoma Cancer

Non melanoma cancer are the most common skin cancer diagnosed all over the world. It generally develops on top layer of skin called epidermis. Basal Cell

Carcinoma (BCC) and Squamous cell carcinoma (SCC) comes under the non melanoma cancer and discussed in detail.

A. Basal Cell Carcinoma

BCC constitutes the 80% of all non melanoma cancers and generally occur on face, head and neck. In early stages, it appear as pale pink colured patches and slowly grows into red shiny liquid filled cyst. If not treated early, it may ulcerate and cause damage to nearby skin and bones. Some image examples are shown in figure 6. It is very rare that these cancer cell metastatize and thus can be treated completely if diagnosed at an early stages.

(a) (b)

Fig. 6 Basal Cell Carcinoma located at a) face b) ear

B. Squamous Cell Carcinoma (SCC)

About 20% of non melanoma cancer consists of SCC and occurs in only epidermal layer. It develops in head, face, lips, ears, legs and feet. It can grow deeper into the layers and may spread to other parts of body. Some image examples are shown in figure 7. It can be easilty treated and completely removed from skin. Sometimes, it originates from actinic keratoses, precancerous condition caused due to prolonged exposure to sun.

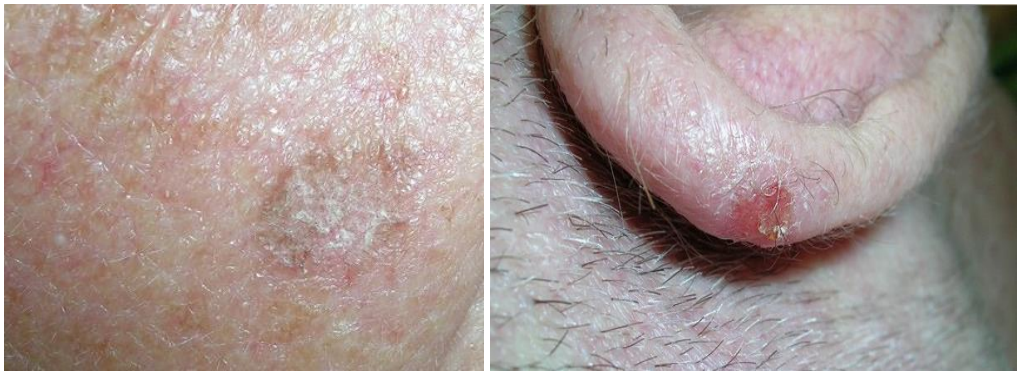

Fig. 7 Squamous Cell Carcinoma

C. Seborrheic keratoses

Seborrheic keratoses (SK) appeared as tan, brown and black spots on skin. It has a waxy texture and raised structure as shown in figure. They are benign and cannot metastatize. It appear on face, chest and back and usually cause no harm. Sometimes, no treatment is needed. But, it is very difficult to differentiate between sk and melanoma.

Fig. 8 Seborrheic keratoses

2.3.2 Melanoma Cancer

Melanoma cancer is rarely diagnosed but most dangerous among all skin cancers. It develops in chest, back and legs. Some instances showed that it may develop in eye, mouth and genital area. It is very difficult to differentiate between nevus and melanoma skin cancer. The color of these lesion depend whether the cell form melanin or not, if melanin are formed then it appear as dark else pink. Some image examples are shown in figure 8. Melanoma cancer can metastatize to different part

and cause damage to other organs. The study conducted by American cancer society showed that majority of deaths are caused due to melanoma cancer.

Fig. 9 Melanoma Cancer

CHAPTER-3

COMPUTER AIDED DIAGNOSTIC SYSTEM

3.1 HANDCRAFT BASED CAD SYSTEM

The handcraft-based CAD system employs predictive machine learning models like decision trees, regression techniques, and SVM for classification. The generic architecture shown in figure 10 below has two phases: detection phase and classification phase. The detection phase includes image acquisition, image preprocessing, and image segmentation, whereas classification consists of steps involving feature extraction, feature selection, and classification.

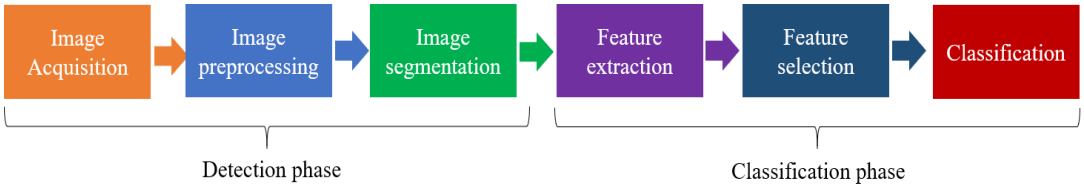

Fig. 10 Flow chart of handcraft-based CAD system

3.1.1 IMAGE ACQUISITION

Image acquisition was one of the essential tasks of the CAD system. Many imaging techniques are evolved during the past decade, which includes camera photography, dermoscopy[5], confocal microscopy (CM)[6][7], ultrasound[8][9], magnetic resonance imaging (MRI)[10][11], optical coherence tomography (OCT)[12], and multispectral imaging[13][14]. The key points of each of these techniques, along with their merits and demerits, are illustrated in table 1.

Table 1: Overview of different image acquisition techniques

Imaging methods	Detection level	Keypoints	Advantages	Disadvantages
OCT	Tissular level	- Highlight the axial section of tissue. - Measure scattering, absorption, birefringence.	- It captures at a resolution of a few µm and to the depth of 1–3 mm. - It is a noninvasive technique	- It requires expert knowledge to analyze such images. - Not enough data to measure its

Imaging methods	Detection level	Keypoints	Advantages	Disadvantages
			capturing enhanced contrast and color features.	effectiveness and thus not recommended for clinical use.
Confocal Microscopy (CM)	Cellular/ subcellular level	- The latest CM system provides higher resolution than routine histology (µm level axial and sub µm level lateral resolution). - Measure depth of melanocytic invasion.	- It is a noninvasive method that evaluates longitudinal morphological features. - It captures the depth of invasion and evolution parameters.	- It is limited to 250µm deep tissue. - There is no biological information related to the state of cancer. - The grayscale contrast lacks specificity.
ELM	Cellular	- A cross-sectional survey of skin lesions under a dermatoscope is performed. - New generation dermatoscope use polarized light and provide fast and enhanced results.	- It significantly improves the distinction between non-melanoma and melanoma cancer. - It minimizes the false-negative results.	- It provides low-resolution images.
MRI	Cellular level	- It uses the magnetic property of the proton and generates high-resolution images(<100µm).	- MRI provides an accurate measure of the depth of invasion. - It is the most	- It has very low sensitivity. - It requires a large scanning time to

Imaging methods	Detection level	Keypoints	Advantages	Disadvantages
		- It provides soft tissue contrast that helps in studying abnormalities in skin lesions. - It helps in evaluating the therapeutic response of melanoma.	efficient way of detecting the shape, size, border, and area of spread of skin cancer.	generate series of images. - Melanoma shows T1 hyperintensity .
Fluorescence spectroscopy	Molecular-level	- It detects the biochemical constituents of skin lesions. - It performs a Quantitative measurement of specific chromophore tissues.	- It establishes a relationship between fluorescent intensity and the proliferation of disease. - Morphological and pathological changes are easily observed.	- This technique is unable to provide a graded diagnosis of cancer
Raman Spectroscopy	Molecular-level	- It uses a Raman microscope to study the vibrational energy of molecules. - The spectrum consists of peaks that correspond to a specific molecule.	- High sensitivity towards biochemical changes. - It is swift and can be used to observe tissue at different depths.	- Skin redness due to exposure to the sun affects the results.
Ultrasound	Lymph	- High-frequency	- It helps in	- It doesn't

Imaging methods	Detection level	Keypoints	Advantages	Disadvantages
	nodes	sonography(20MHz) and mid-range frequencies (7.5-15MHz) are used for scanning internal structures of skin lesions. - It detects the malignant and benign cancerous tissue.	diagnosing lymph nodes affected by cancer. - Ultrasound contrast agents can improve the specificity of diagnosis. - It is handy in surgical planning.	correctly diagnose the small tumor and can't be used independently for early diagnosis. - The location of the tumor may also affect the results.

3.1.2 IMAGE PREPROCESSING

Images acquired from the different image acquisition techniques consist of several artifacts like hair, dermoscopic gel, blood vessels, and trapped air bubble, which compromise the CAD system's accuracy. The image preprocessing technique removes these artifacts and noises by applying filter transformation on each image. The most commonly used filters are the Median filter[15][16], Gaussian filter[17][18][19], anisotropic diffusion filter, and mean filter. Jaleel et al. [20] apply a fast median filter to remove noises and a "Dull Razor" app to remove hair from images. However, these methods are quick but simultaneously dilute the lesion's borders with the surrounding skin (see Fig. 11) and thus pose a challenge to capture border details. Specific algorithms are proposed to grab border-related artifacts that utilize contrast stretching [20] and sharpen the images.

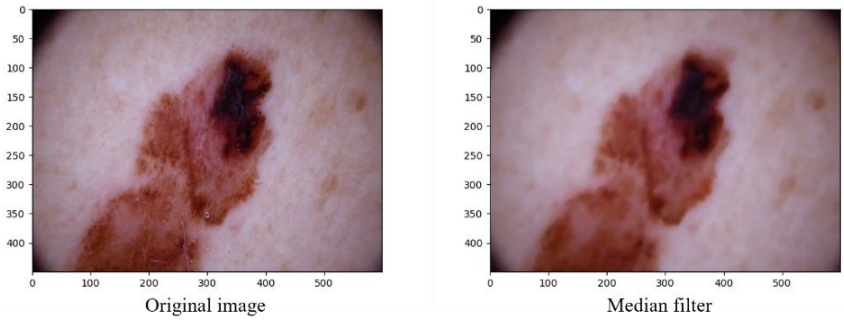

Fig. 11 Noise removal using median filtering

Skin lesions consist of a pigmented area with multiple color shades. Thus, one of the efficient techniques employed color quantization and color space transformation [21]. In color space transformation, an original image RGB color coordinates are mapped to secondary color space such as CMYK (Cyan, Magenta, Yellow, Black) and device-independent color space such as CIEL∗a ∗b, etc. These transformation techniques would further help in image segmentation. However, these techniques successfully remove artifacts like blood vessels and skin lines, but some dermoscopy images have scale lines and other geometrical shapes requiring attention. M.G.Fleming et al.[22] employed top hat operator to remove bubbles and bright edges. Q. li et al.[23] utilizes derivatives of gaussian (DoG) to removes the scales and lines.

3.1.3 Image Segmentation

The enhanced images obtained after preprocessing were segmented to generate a mask. Skin lesion areas are extracted from the original image with the help of these generated masks. The accuracy of any CAD system depends on how precisely it segments the pigmented region from a given image. Many segmentation techniques were proposed, such as thresholding techniques, regional and texture-based segmentation.

Segmentation using thresholding techniques includes histogram thresholding, adaptive thresholding. These methods employed on monochrome images and pixel values less than specified threshold belong to one class and otherwise belong to another category. It may be bi-class or multi-class thresholding. Otsu's algorithm is an efficient way of segmenting a filtered image, and much literature used this method to segment skin lesion areas. The output mask generated by otsu’s algorithm is shown in Fig 12. Jaleel et al. [20] employ

maximum entropy-based techniques and calculate the mean of skin lesion image entropy and selected threshold to maximize the entropy.

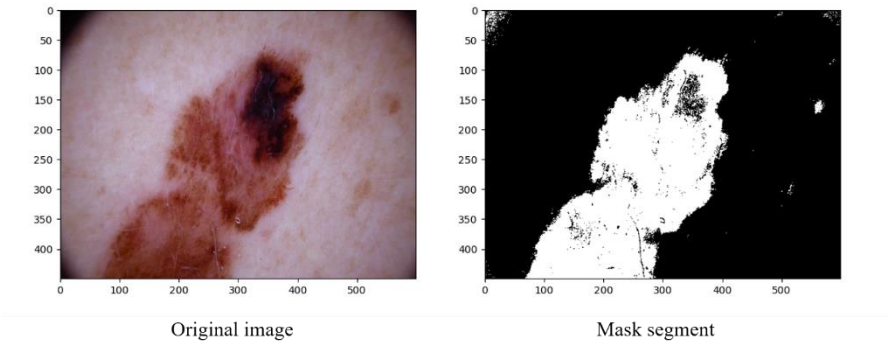

Fig. 12 Image segmentation using Otsu's algorithm

Region-based segmentation defines certain regions using homogeneity criteria. Some of the standard techniques include seeded area growing, watershed algorithm, and morphological flooding techniques. The segmentation result after performing the watershed algorithm are depicted in Fig.13 below. However, much shreds of evidence show these methods didn't produce satisfying results. The most prevailing practices nowadays use different texture-based segmentation methods to generate a cluster of pigmented skin lesions. V. Shrividaya et al. [24] segment the background and foreground texture details using a suitable mask. Shoieb et al. [15] computes multi-resolution decomposition using Gabor filters and applying K-means clustering to cluster a region with similar textures. This approach shows promising results but computationally expensive. Fuzzy C-means approach proposed by Celebi et al.[16]and Rehman et al. [25] introduced fuzzy logic to segment the image. However, this method is insensitive to noise but does not include spatial data.

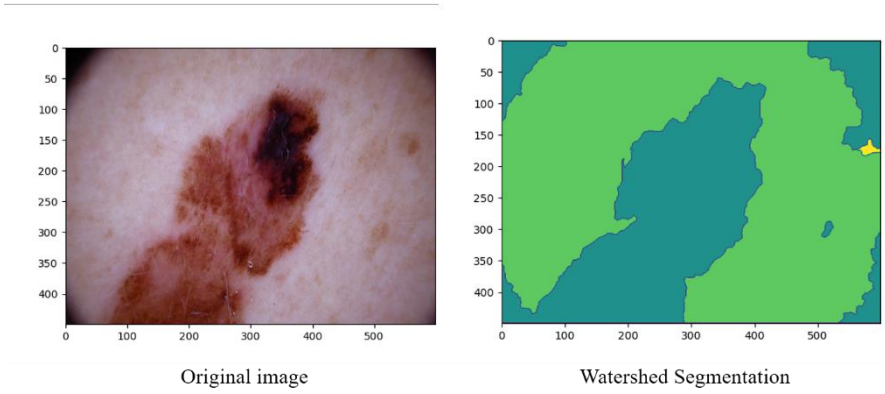

Fig. 13 Region-based segmentation using watershed algorithm

3.1.4 Feature Extraction

The next critical step in detecting skin cancer is feature extraction. Feature extraction involves feature detection and description from a segmented image. The segmented region has some attributes related to it, such as area, contrast, energy, symmetry, and several statistical, geometrical, and textural features, which should be abstracted and described using feature descriptors to facilitate the classification process.

Statistical features include the mean, median, kurtosis, standard deviation of the histogram of images. Geometrical features consist of diameter, circularity etc. Monika et al.[26], proposed a standard method to detect features such as asymmetry, border irregularity, color, dimension of a patch, and evolution (ABCD-E). These feature vectors are calculated from different feature descriptors, like area of patch provides information about symmetry such as if patch divided into two half and area of both halves are equal then it is symmetric so comparison of the area will be a feature descriptor. Similarly, the eccentricity and maximum distance between two pixels will define border regularity and evolution. However, the sensitivity achieved by the ABCD method was only 77.55% [27]. Dermatologists used some alternative approaches such as the Menzies method [28] and 7-point checklist [29] to extract features and achieved 84.6% and 81.4% sensitivity [27].

In addition to these methods, some techniques evaluate features using frequency-domain transformation and filtering, such as wavelet transform, Fourier transforms, and gaussian derivatives etc. O Abuzaghleh et al. [30] utilizes 2-D FFT, 2-D DCT to extract features and also include color features. Color-related features include maximum and minima of intensities, HSV values etc., of the pigmented region, have also found many applications in CAD systems. Shoieb et al.[15] incorporates Gabor wavelets filter on an input image and converted image intensities value as features. Maglogiannis et al. [17] demonstrate gray level co-occurrence matrix (GLCM) technique to extract texture-based features vector.

3.1.5 Feature Selection

The primary objective of feature selection is to select a set of features to perform the classifier model better. Features significantly impact our predictive model as learning on irrelevant features will lead to inaccurate results [31]. It also helps the model to avoid overfitting. Second, in feature selection, performing PCA and

finding a correlation between features decides how many features to be included for prediction. Therefore, reducing feature space which significantly reduces the training time and complexity of the prediction model.

Generally, feature selection is classified into supervised and unsupervised feature selection. Supervised feature selection includes filter-based selection, wrapper techniques [32]. Feature selection procedures are characterized by their generation procedures and evaluating function. In Table 2, different feature selection methods and their corresponding generation procedures and evaluation function. The wrapper feature selection method utilizes many models trained on different subsets of features and selects those features which have given the best performances [32]. However, it is computationally expensive, and only a greedy search is applied. Moreover, the solution is not optimal and sometimes undergoes false starts. In filter-based feature selection, a particular statistical relationship between input features and output classes is established and based on their results; one can filter out relevant features [33]. Redundant features may be included, which might not be suitable. Another disadvantage includes negligence of features that may not perform well independently but provide good results commutatively. Feature selection procedures are characterized by their generation procedures and evaluating function.

Table 2: Illustration of different feature selection methods and their corresponding generation procedures and evaluation function

Feature selection method	Generation procedures	Evaluation function
Relief and its variants	Heuristic	Distance
Branch and Bound(B&B), BFF	Complete	Distance
Decision tree, and Koller and Sahami's method	Heuristic	Information
Minimum Description Length Method (MDLM)	Complete	Information
Probability of ERROR & Average Correlation Coefficient, PRESET	Heuristic	Dependance
Focus, and Schlimmer's method, and MIFES 1	Complete	Consistency
LVF	Random	Consistency
SFS, SBS, SBS-SLASH, POSS, BDS, Schemata Search, relevance in context (RC), and Queiros and	Heuristic	Classification error rate

Feature selection method	Generation procedures	Evaluation function
Gelsema's method		
Beam search, AMB&B, Ichino and Sklansky method	Complete	Classification error rate
Genetic algorithm, LVW, RGSS, RMHC-PF1	Random	Classification error rate

3.1.6 Classification

CAD systems usually classify pigmented skin lesions into one of the seven categories. In contrast, some CAD systems are used to classify the skin lesion into malignant (melanoma) and benign. There are many classification algorithms employed on the features selected at prior stages. Some of the existing methodologies include K-nearest neighbors (KNN)[34][35][36], support vector machine (SVM), decision trees (DT)[37][38][39], Bayesian networks, ANN, and extreme learning machine (ELM).

1) Logistic Regression

Logistic regression is a supervised statistical algorithm that is used for multi-class regression and classification problems. It generates a linear hyperplane or decision boundary among different classes by solving a set of equations derived from training data. However, this model is straightforward to implement, but it could not produce non -linear decision boundary. Burroni et al. [40] proposed a supervised machine learning approach to classify dermoscopic images into in-situ melanoma and dysplastic nevi. A set of 48 features are selected, including textures, color, and geometrical features from ×16 magnified images. Multivariate logistic regression is used as a classifier and achieved 71.8% of accuracy.

2) *K Nearest Neighbours (KNN)*

KNN is a non-parametric pattern recognition method that determines a new sample class based on k nearest neighbors. In this algorithm, a parameter k is statistically calibrated to increase the accuracy of the classifier. The algorithm's first step is to select k nearest samples values from the dataset distribution, followed by calculating Euclidean distance or Manhatten distance of these

neighbor samples with the test sample. Then segregate the number of samples belonging to a specific category. Finally, the class having the maximum number of neighbors would consider as the category of a sample under test. Selection and segregation of samples are prolonged if the number of neighbors increases. This algorithm's major drawback is that if the dataset imbalance is present, it is biased concerning output. It is also sensitive to outliers.

Ramlakhan et al. [35] proposed an automatic detection of skin cancer for mobile applications. The work is composed of image segmentation using otsu's method shapes color and texture features extraction and classification using the K-NN classifier. It achieved an accuracy of 66.7%. Although the methodology proposed cannot achieve great results, but the computational cost is high. Results suggested the introduction of several other features may improve the classification rate.

Burroni et al. [36] perform classification of melanoma and benign pigmented skin lesion using KNN classifier and achieved significant results. A Laplacian filter with zero-crossing thresholding is utilized to perform the segmentation of images. Moreover, a set of 19 features are extracted, including border irregularity, mean skin lesion gradient, mean contrast, and entropy of lesion, which helps to achieve a misclassification rate of 12.5%, 98% of sensitivity, and 78% specificity.

3) Decision Tree

The decision tree is a popular technique used for regression and classification of skin cancer detection. Decision tree constructs tree based on features extracted. Entropy and information gain of features are regarded as criteria to select root nodes and splitting the tree. The final level consists of leaf nodes which represent classes or categories. A decision tree will undergo overfitting if the dataset is large. Decision tree pruning is done to avoid overfitting. It involves identifying subtree that contributes less to predictive accuracy and replaces by a leaf node.

Decision trees were frequently used to detect blue-white veils and classify veil and non-veil nevus. Celebi et al. [37] noticed the blue-white veil and its related structures on dermoscopy ATLAS dataset using decision tree and achieved 69.35% sensitivity and 89.97% specificity. It classifies the lesion as benign or melanoma based on an area of the blue-white veil. Patwardhan et al. [39] proposed an adaptive wavelet-based tree algorithm to distinguish melanoma

images from dysplastic skin lesion images. It introduces feature vectors defining average energy and energy ratios of four sub-images and adaptive thresholding for splitting trees. The model achieved a 90% true positive and 25% false-positive rate.

4) Support vector machine (SVM)

SVM is an efficient and powerful supervised learning method used for regression and classification problems. SVM systems utilize kernel trick to transform the input features to higher dimensional space to find non-linear decision boundaries. The maximal marginal hyperplane is calculated using statistical learning theory to minimize expectation error (see Fig. 14). Kernel function plays a significant role in the performance of SVM. Linear, polynomial, Gaussian, and exponential radial basis functions are commonly used kernels in SVM. Dreiseit et al. [34] perform a comparison of different SVM models for classifying melanoma from common and dysplastic nevi. The results suggest that the RBF kernel SVM model outperforms polynomial kernel SVM.

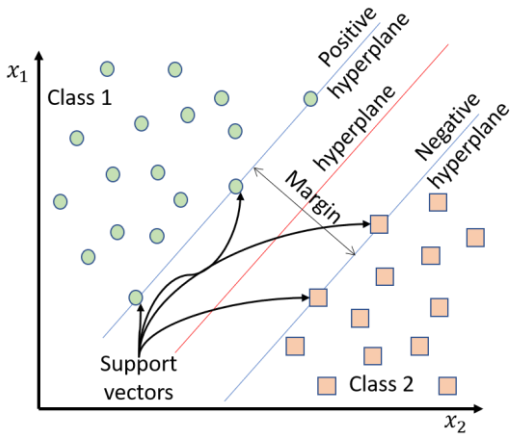

Fig. 14 SVM model

Gilmore et al.[41] uses SVM to classify melanoma and dysplastic skin lesion and achieved significant results. In this work, a set of 14 features are selected, including color and asymmetry attributes, and trained using RBF kernel. The methodology achieved 86% of sensitivity, 72% of specificity, and AUC of 76%.

Yuan et al.[42] proposed a texture-based identification of benign and malignant melanoma using SVM. The model extracted features from Gabor filtering and local autoregression and trained using SVM with the polynomial

kernel. The work demonstrates that error increased after the 4th order polynomial kernel and achieved an accuracy of 70%.

Rehman et al.[25] perform segmentation and classification of skin lesion images. Fuzzy c means and iterative thresholding are used to segment images and further extraction of color and texture-based features using covariance matrices. Later, classification using SVM is performed using a different kernel. The result demonstrated that SVM with RBF kernel performed well and achieved 70.9% of accuracy.

5) Artificial Neural Network(ANN)

ANN is a powerful predictive model whose architecture development is inspired by a human brain. As shown in Fig. 15, the basic architecture of ANN consists of an input layer, hidden layers, and an output layer. The hidden layer consists of nodes that take a weighted input and apply the activation function and generate activated output. Every node of one layer is connected to each node of the next layer. Generally, the ReLU activation function is used at the hidden layer and the softmax function at the output layer. The weights are automatically adjusted to reduce loss function by backpropagation. Moreover, ANN produces a significant result in classification problems. However, it found many applications in medical analysis, their performances based on the amount of training data.

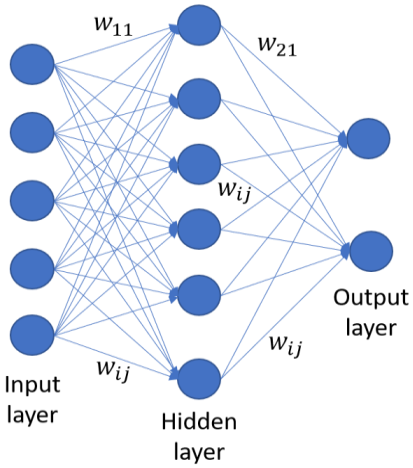

Fig. 15 ANN architecture

3.2 CNN BASED CAD SYSTEM

The emergence of deep learning and computer vision has led to a more advanced CAD system for detecting skin cancer diseases. CNN-based CAD system has

shown noticeable results in medical image applications. CNN-based CAD methodologies involve automatic feature extraction through a different layer of CNN. The performance of CNN and deep learning methods depend on datasets used to train the model. The popular benchmark datasets are explained briefly. The study of different architectures proposed recently can be divided into two groups segmentation and classification task. We present a brief survey of all the recent works published to segment skin lesion images in the segmentation task sub-section, and elaborated the studies related to pigmented skin lesion image classification in the classification task sub-section.

3.2.1 CNN Overview

CNN architecture developed to overcome the demerits of artificial neural networks for image analysis, such as loss of spatial information. It consists of three fundamental features that reduce the parameters in neural network spatial interaction, parameter sharing, equivariant representation. CNN creates spatial features, say we have an image which after passing through a convolution layer gives rise to a volume then a section of volume taken through depth will represent features from the same part of the image furthermore each feature in a depth layer generated by the same filter that convolves image. CNN consists of layers classified into a convolutional layer, activation layer, pooling layer, fully connected layer(FC), and softmax layer. Some fundamental architecture of CNN includes LeNet, AlexNet, and VGG, whereas more complex and efficient architectures proposed by researchers include GoogLeNet, ResNet and DenseNet. Convolution and pooling are the fundamental operations that are used to filter sparse features. These features are flattened using FC layers, and classification is performed at the last output layer. Output layer uses a sigmoid and softmax function to perform binary and multi-class classification, respectively.

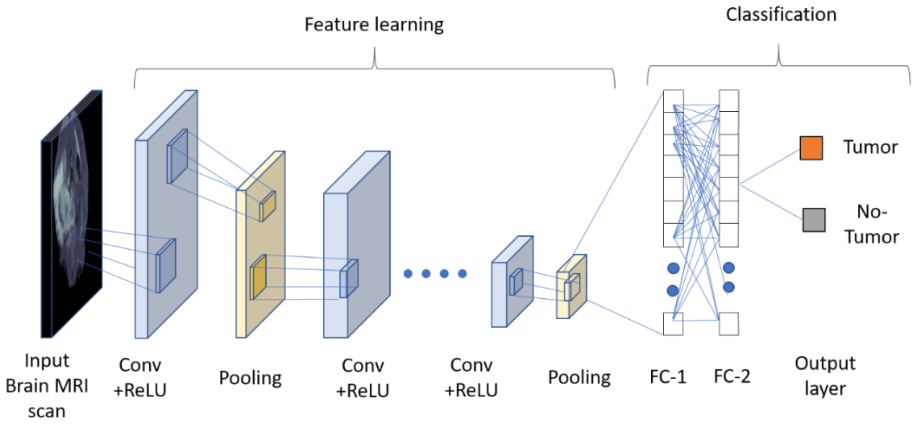

Fig. 16 Basic CNN Architecture

Depth, filter size, activation function, and optimization functions are some parameters that affect the performance of the CNN model, and the number of trainable weights decides its memory storage requirements. The memory requirements generally increase as the depth of the network increases, but it was observed that many advanced architectures introduce bottleneck architecture and smaller filter sizes to reduce trainable parameters and memory size. However, some CNN models are computationally complex, such as DenseNet but perform well on large datasets. In Table 3, all the famous state-of-art CNN models proposed and also the models that won the ISLRV competition are enlisted with their key points.

Table 3 Overview of State-Of-The-Art CNN Architectures

Authors	***CNN Architecture***	***Year***	***Keypoints***
Lecun	LeNet	1998	- The seven layers deep architecture is proposed to learn features from an image automatically. - The network consists of a pair of convolution layers and sub-sampling layers, followed by FC layers and an output layer. - It uses Tanh as an activation function. - The model reduces the error rate using backpropagation which makes this model adaptive.

Authors	***CNN Architecture***	***Year***	***Keypoints***
Krizhevsky	AlexNet	2012	- It consists of 5 convolutional layers, 2 FC layers, and an output layer for classification. - It uses ReLU as an activation layer and performs local response normalization after the first and second convolution layers. - It employs heavy data augmentation and also uses a dropout of 0.5. - The network is learned with SGD momentum.
Zeiler	ZFNet	2013	- ZFNet model used improvised hyperparameters of AlexNet. - It utilizes a smaller kernel size and more filters. - Introduces a concept of capturing greater receptive area using smaller kernel size while reducing the number of parameters.
Szegedy	GoogLeNet	2014	- It is 22-layer deep that incorporates computational efficiency using a stack of inception modules. - No fully connected layer. - It has 12 times less number of a parameter as compared to AlexNet. - The inception module applies parallel filtering using Convolution, having different filter sizes and pooling followed by concatenation. - The computation complexity increases.

Authors	***CNN Architecture***	***Year***	***Keypoints***
Simonyan	VGGNet	2014	- Depth of VGG Net is more as compared to AlexNet. - It has three variants, VGG-11, 16, and 19, comprised of 8, 13, and 16 convolution layers. - It achieves the same effective receptive field by stacking smaller filer sizes that a larger filter can cover. - It introduces more nonlinearity than AlexNet while reducing the number of parameters.
He	ResNet	2015	- It introduced an immensely deeper network and used residual connection. - It stacks residual blocks, and each block consists of two 3×3 convolutional layers. - It implements batch normalization after Convolution and before pooling. - It has overcome the vanishing gradient problem.
Xie	ResNeXt	2016	- It is similar to ResNet but introduces cardinality(number of paths) and replaces residual block with ResNeXt block. - A ResNeXt block consists of a multi-path network each operates on segregated data. - It incorporates three convolutions of having kernel size 1×1, 3×3, and 1×1 in every branch to extract different features and merge every branch output to obtain the final feature map.

Authors	*CNN Architecture*	*Year*	*Keypoints*
Huang	DenseNet	2017	- It incorporates an idea of feature reuse which results in compact architectures. - It utilizes dense blocks in place of residual blocks. - Within each dense block, every convolution layer concatenates with the previous layer input by skip connections. - It alleviates vanishing gradient problems. - A shallower model with dense block outperforms deep residual networks. Thus, it reduces the memory size requirement and the number of trainable parameters.
Howard	MobileNet	2017	- It has a class of efficient models designed for mobile applications. - Critical ingredients of architecture are depthwise separable Convolution. - Standard Convolution is replaced with depthwise Convolution followed by pointwise (1×1) Convolution. - Every convolution layer is followed by batch normalization and ReLU activation layer. - It considered two hyperparameter width multiplier(α) and resolution multiplier(ρ) to control the number of channels and scaling of an input image. - This model has a small size and low latency.

Authors	*CNN Architecture*	*Year*	*Keypoints*
Tan and Le	Efficient Net	2019	- It introduces a concept of compound scaling of an architecture. - It scales the baseline architecture depth, width, and input resolution using a single coefficient. - It achieves better performance at a lower depth than ResNet and other models. - It maximizes the use of available computational resources while fulfilling the desired performance matrices.
Alexander	BigTransfer (BiT)	2020	- It is a scalable ResNet model means utilizes more channels at each layer of Convolution. - It is trained on the JF dataset, and this pre-trained model is used for other image classification tasks. - The major contribution involves the use of Group Normalization and Weight standardization in place of the Batch Normalization layer. - Studies showed that this pre-trained model works well on a small dataset.

Comparison of State-of-the-art CNN

The parametric analysis of CNN models based on Top1 accuracy, Top 5 accuracy, image size, filter size, the number of trainable weights, and multiply and addition operations (Mul-Add) is illustrated in Table 4.

Table 4 Comparison of state-of-the-art CNN architectures

Model / *Parameters*	*LeNet-5*	*AlexNet*	*ZFNet*	*VGG-16*	*GoogLeNet*	*ResNet-50*	*DenseNet*	*MobileNet*	*Efficient Net(B7)*
Top 5 accuracy(%)	-	84.6	84.0	91.9	93.7	92.1	92.3	89.5	91.7
Top1 accuracy(%)	-	63.30	-	74.5	69.8	78.25	77.85	65.14	84.80

Model / Parameters	*LeNet-5*	*AlexNet*	*ZFNet*	*VGG-16*	*GoogLeNet*	*ResNet-50*	*DenseNet*	*MobileNet*	*Efficient Net(B7)*
Input size	28×28	256×256	224×224	224×224	224×224	224×224	224×224	224×224	224×224
Filter Size	[5×5] & [2×2]	[11×11], [5×5] & [3×3]	[7×7] & [3×3]	[7×7] & [3×3]	[1×1], [3×3], [5×5] & [7×7]	[1×1], [3×3] & [7×7]	[1×1], [3×3] & [7×7]	[1×1]& [3×3]	[1×1], [3×3], & [5×5]
Stride	1, 2	2,4	2	1	1,2	1,2	2	1, 2	1,2
FC layers	2	3	3	3	n/a	1	n/a	1	1
Trainable Weights	432K	61M	n/a	138M	7M	25.5M	15M	4.2M	66M
Mul-Add	2.3M	724M	n/a	15.3G	1.42G	3.91G	2.12G	569M	-

3.2.2 Related work for skin lesion Segmentation

Yuan et al.[43] proposed a convolution and deconvolutional neural network to segment skin lesion images. The proposed model consists of 29 layers, including convolution layers, pooling layers, deconvolution layers, and upsampling layers. Data augmentation like scaling and rotation is used to increase the number of training samples and avoid overfitting of the model. The model trained on the dataset provided by ISBI challenge 2017. The dataset consists of 2000 dermoscopic images. A binary mask is generated using the model and achieved an average Jaccard index of 0.7.

In [44], a multi-input CNN model is proposed for pixel-wise segmentation. Local patch and global patch sub-images with the same center pixel location are fed to two parallel convolution layers followed by the pooling layer. The local and global features extracted from patches are then connected at a fully connected(FC) layer. Finally, predict the pixel as a lesion or normal skin using the softmax layer. The Dermquest dataset was a benchmark for the work. Moreover, resizing the image to 600×400 pixels and patches of size 31×31 are selected to train the model. It achieves an accuracy of 98.5%, 95% sensitivity, and 98.9% specificity.

In [45], a full resolution convolution network (FrCN) is presented to segment skin lesions in dermoscopic images. In this work, ISIC-2017 and PH2 datasets are used separately. In the experiment, a CNN model having a baseline architecture of VGG 16 without any sub-sampling layer (pooling layer) is used. Each fully connected layer is replaced by Conv. layer at the output side. This method took only 9.7s to segment an image of size 192×256 pixels. The proposed methodology achieved a Jaccard index of 77.11%, an accuracy of 94.03%, a

sensitivity of 85.4 %, and a specificity of 96.9% for the ISBI 2017 dataset and 84.79% Jaccard index, 95.08% accuracy,93.72% sensitivity, and 95.65% specificity for PH2 dataset.

In [46], a novel approach using Dense Deconvolutional Network(DDN) is introduced. The model includes the encoder and decoder phases for semantic segmentation of images. The encoder employs ResNet architecture, whereas the decoder involves residual block, chained residual pooling layer, and dense deconvolution layer to capture hierarchical features. It performs training on the ISBI 2016 and 2017 datasets consisting of 1179 images. The proposed approach has achieved significant results with 87% Jaccard index, 95.9% accuracy, 95.1% sensitivity, and 96% specificity for ISBI 2016 dataset, and 76.5% Jaccard index, 93.9% accuracy 82.5% sensitivity, and 98.4% specificity.

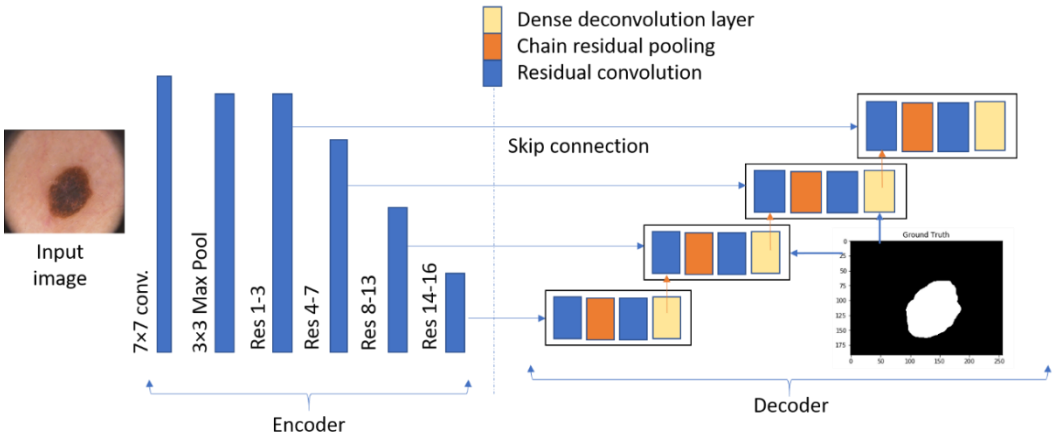

Fig. 17 Overview of the proposed DDN framework in [46]

In [47], an end-to-end framework employing multi-stage UNet is proposed to segment skin lesion images. In the MS-UNets context, information fusion structure (CIFS) was introduced to eliminate the vanishing gradient problem. The probability map of the previous UNet classifier and RGB images is fed to a successive classifier to enhance the predicted output. The model has trained on the ISIC-2016 dataset and achieved 95.87% accuracy, 85.34% Jaccard index, 92.67% sensitivity, and 96.42% specificity.

In [48], a Generative Adviseral Network (GAN) model is proposed to effectively segmentation lesion images. The model consists of skip connection and diluted convolution UNet (UNet-SCDC) with two discriminative blocks, which reduces the error between segmented output and ground truth. The network was able to generate dense features and preserve fine-grained information. The model is

trained on the ISIC-2017 dataset consist of 2000 dermoscopic images. This approach outperforms many previous state-of-the-art segmentation techniques. It achieved an accuracy of 89.6%, 85.9% of sensitivity, 91.0% specificity, and 73.4% of the Jaccard index

.

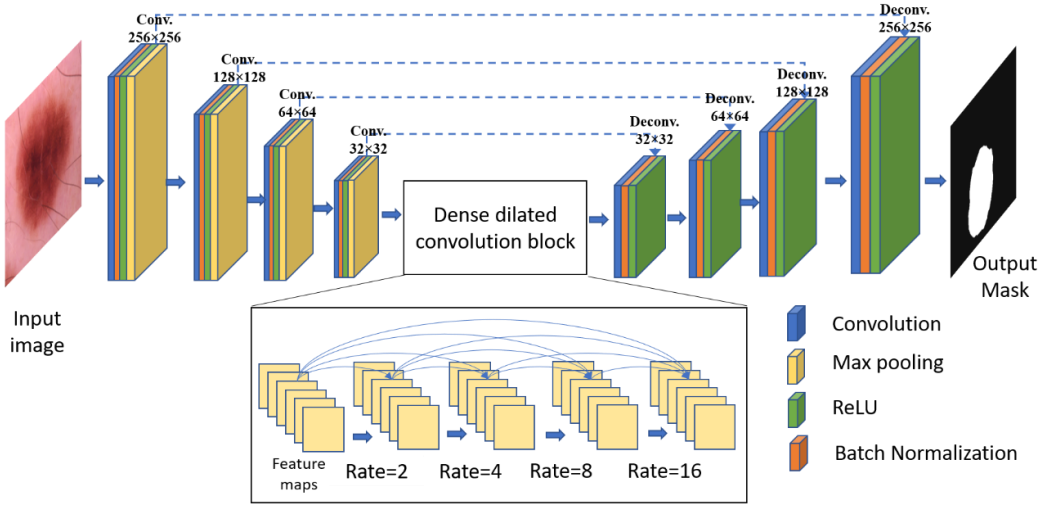

Fig. 18 Overview of UNET-SCDC architecture for segmentation of an image

In [49], implements U-Net architecture to generate the binary mask. The architecture performs well in many segmentation tasks. In this work model, training was performed on ISBI 2015 dataset and achieved an accuracy of 91.8%, 70.5% of Jaccard index, 97.8% of specificity, and 77.7% of sensitivity.

In [50], a new loss function is proposed, which utilizes star-shaped prior information. This loss function is used to train the FCN model and optimized using a stochastic gradient descent algorithm. The model has a baseline architecture similar to ResNet-DUC that enhanced the segmentation task of skin lesion images. The experiment is performed on ISIC 2017 dataset. Finally, an accuracy of 93.8%, 85.5% of sensitivity, specificity of 97.3%, and Jaccard index of 77.3% is achieved.

In [51], a Fully convolutional network framework is proposed to perform semantic segmentation on images. The major advantage of this network is that it operates on the input of any size. This model performs well on the ISBI-2017 dataset. The approach achieved an accuracy of 92.72%, specificity of 96.66%, Jaccard index of 72.17%, and sensitivity of 79.98%.

In [52], an unconventional approach that utilizes a Multi-scale convolutional network (MSCN) is proposed. This approach uses different scaled features and recognizes low-contrast objects. The shapes of the cell are estimated

using the gaussian kernel. It has experimented on ISBI 2015 Challenge Dataset and Shenzhen University (SZU) Dataset. Although the method addresses overlapped nuclei, it takes more than 12 minutes to analyze a 1360×1024 pixel image.

3.2.3 Related work for Melanoma classification

In [53], the AlexNet model is trained on low-resolution dermal images taken from Panasonic Lumix FZ-35. Data augmentation is also included to generalize the model and achieved an accuracy of 96%. However, this technique performs well on low-quality images. It will not produce significant results when trained on high-resolution dermoscopic images.

In[54], models based on VGG16 are used to classify skin lesion images of the ISBI 2016 challenge dataset. The model is tuned by training top layers of architecture and freezing other layers. The methods enhance the conventional CNN performances and achieved 81.33% accuracy and 78.6% sensitivity.

In [55], employed a pre-trained ResNet 50 architecture for classifying skin lesion images. ISIC 2017 datasets are used for training purposes and also utilize data augmentation techniques to increase training data. In this experiment, two parallel architectures are used to train dermoscopic images and macroscopic images. The FC layers' output is concatenated with metadata of patients to build a multimodal architecture to classify the images. It achieved an AUC of 85.8%.

Singhal et al.[56], presented a comparative analysis of popularly known state-of-the-art CNN models for skin lesion classification tasks. In this paper, transfer learning is implemented using pre-trained models Inception v3, ResNet 50, DenseNet 201, and Inception ResNet v2 on the HAM10000 dataset. The overall accuracy of Inception ResNet v2 is 81.62%, and that of DenseNet is 81.425. Some other valuable insights include that DenseNet achieved the best macro average AUC.

In [57], a multi-scale multi-network ensemble of pre-trained CNN models is introduced to classify skin lesion images. It incorporates a three-level fusion method. Efficient Net B0, Efficient Net B1, and SeResNext-50 are trained on images having fixed sizes using five-fold cross-validation. At the second level, the prediction vector of these submodels is fused with models trained on images of different sizes, and finally, they are all combined to give one model. It achieved a

balanced multi-class accuracy of 86.25% in ISIC 2018 challenge and outperformed many other methodologies.

In [58], proposed a methodology to detect skin cancer and typical skin images using a deep learning approach. In this work, five deep learning model, including ResNet, SqueezeNet, and DenseNet is implemented, and their performances on HAM 10000 dataset are compared. It achieved an average AUC of 99.1%. Results concluded that model build using deep learning studio provide better than the conventional models.

Yao et al.[59] proposed a deep convolutional neural network(DCNN) with a novel approach for data augmentation and loss function. Modified RandAugment augmentation techniques help the network to overcome the class imbalance problem of the dataset. Moreover, a multi-weighted confocal loss function is introduced to achieve high classification accuracy. The methodology was implemented on ISIC 2018 challenge dataset and achieved an average multi-class accuracy of 86.4%, 77.2% sensitivity for melanoma class.

In [60] proposed a hybrid CNN model to classify the skin lesion into seven classes. It incorporates three pre-trained CNN models AlexNet, VGG 16, ResNet18, to extract features that will further used to train the SVM classifier. The classification results were evaluated on ISIC 2017 dataset, and data augmentation was also employed to increase performance. The model achieved an accuracy of 90.69%.

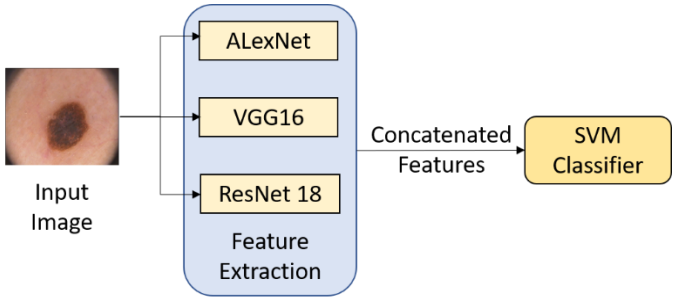

Fig. 19 Hybrid CNN Model

In [61], different hybrid CNN classifiers are proposed, and a comparative analysis of their performance on the PH2 dataset and ISBI-ISIC dataset consists of more than 1000 images are performed. CNN architectures such as VGG, Inception, Res Net, Inception-ResNet, Xception, MobileNet, DenseNet, and NASNet are regarded as feature extractors. The outputs vector of the layer preceding the output layer is treated as feature vectors, which are used to train five

classifiers: Bayes, SVM, ANN, KNN, and Random Forest. Their performances are evaluated and compared. The results concluded that these hybrid networks perform well for classifying skin cancer images.

In [62], an ensemble approach employing different CNN architectures for the classification of skin cancer is proposed. It implemented 13 famous states of art methods and then suggested two ensemble techniques. The first method ensemble of all these methods is used to classify skin lesion images, while in another ensemble method, the weighted average of the three best classifiers is used for classification purposes. The architecture implemented on the ISIC 2019 challenge dataset and first ensemble achieves 88.3% accuracy, 98.8% of AUC, similarly 89.7% accuracy, and 98.9% of AUC by the second one.

Table 5 Overview of recent work of DL methods for skin lesion image segmentation and classification. Segmentation(s), classification(C), dice coefficient (DI), accuracy (ACC), sensitivity (SE), specificity (SP), precision (PR), F1 score (F1), area under ROC curve (AUC), balanced class classification accuracy (BACC), Jaccard Index (JA), classification rate (CR).

Dataset	Task	Year	References	Model/architecture	Remarks
ISIC 2019	C	2019	[11]	CNN	ACC-74.48, Loss-0.69
ISIC 2019	C	2019	[11]	MobileNet	ACC-76.48, Loss-0.64
ISIC 2019	C	2019	[11]	Inception v3	ACC-79.93, Loss-0.669
ISIC 2019	C	2019	[11]	Dense Net	ACC-85.83, Loss-0.69
DermQuest	S/C	2016	[12]	CNN+SVM	ACC-93.75
DermIS	S/C	2016	[12]	CNN+SVM	ACC-94.12
Other datasets	C	2013	[13]	ANN	ACC-88, Loss-0.78
DermIS+ DermQuest	S/C	2020	[14]	Texture based segmentation+ CNN	SE-85.7, identification efficiency-95
Dept. of dermatology university of Vienna	C	2001	[15]	ANN	AUC-96.8, SE-91.43, SP-93.97
DermQuest	S	2016	[16]	Multi inputCNN	SE-95, SP-98.9, ACC-98.5
ISBI 2017	S	2018	[17]	FrCNN	DI-77.11, JA-77.11, MCC-83.22

Dataset	Task	Year	References	Model/architecture	Remarks
ISBI 2017	S	2018	[17]	FCN	DI-83.83, JA-72.17, MCC-79.30
ISBI 2017	S	2018	[17]	UNet	DI-76.27,JA-61.64, MCC-71.232
ISBI 2017	S	2018	[17]	SegNeT	DI-82.09,JA-69.33, MCC-83.22
ISBI 2017	S	2019	[18]	DDN	DC-86.6, JA-76.5, ACC-93.9, SE-82.5, SP-98.4
ISBI 2016	S	2019	[18]	DDN	DC-93.1, JA-87, ACC-95.9, SE-95.1, SP-96
ISBI 2016	S	2018	[19]	MSUN+CIFS+DS	JA-85.34, DI-91.47, SE-92.67, SP-96.42
ISIC 2017	S	2020	[20]	UNet-SCDC	ACC-89.6, SE-85.9, SP-91.0, JA-73.4, DI-83.2
ISBI 2015	S	2015	[21]	UNet	IOU-77.56
ISBI 2017	S	2018	[22]	FCN+star prior info	JA-77.3, DI-85.7, ACC-93.8, SP-97.3, SE-85.5
Other datasets	S	2009	[23]	FCN	ACC-75.9
ISBI2015+SZU	S	2017	[24]	MSCNN	DC-89, TP-92, FN-26
Other datasets	C	2017	[25]	Transfer learning with AlexNet+SVM	ACC-98.67, SP-99.08
ISBI 2016	C	2017	[26]	Transfer learning VGGNet	ACC-81.33, SE-78.66, P-79.74
ISIC 2017	C	2018	[27]	Multi-modal CNN	AUC-85.8
HAM10000	C	2020	[28]	ResNet50	AUC-96
HAM10000	C	2020	[28]	Inception v3`	AUC-97
HAM10000	C	2020	[28]	Inception Resnet v2	ACC-81.62
HAM 10000	C	2020	[28]	DenseNet201	ACC-81.42, MacroAUC-93
HAM10000	C	2020	[29]	ResNet	PR-94.24, F1-94.22, AUC-98.61

Dataset	Task	Year	References	Model/architecture	Remarks
HAM10000	C	2020	[29]	SqueezeNet	PR-97.40, F1-94.57, AUC-99.77
HAM10000	C	2020	[29]	DenseNet	PR-97.51, F1-96.27, AUC-99.09
HAM10000	C	2020	[29]	Inceptionv3	PR-98.19, F1-95.74, AUC-99.23
ISIC 2018	C	2021	[30]	DCNN	BACC-85.88(RegNetY-3.2GF)
ISIC 2017	C	2019	[31]	CNN+SVM	AUC-83.33 for melanoma and average AUC- 90.69
PH2	C	2020	[32]	Transfer learning DenseNet+KNN	ACC-93.16, F1-96.7, R-96.80
ISIC	C	2020	[32]	Transfer learning DenseNet+KNN	ACC-96.8, F1-93.15,R-93.15
ISIC 2019	C	2019	[33]	DenseNet-121	BACC-83.2, AUC-97.4
ISIC 2019	C	2019	[33]	DenseNet-169	BACC-81.1, AUC-96
ISIC 2019	C	2019	[33]	DenseNet-201	BACC-82.1, AUC-96
ISIC 2019	C	2019	[33]	GoogleNet	BACC-81.4, AUC-97.5
ISIC 2019	C	2019	[33]	Inception v4	BACC-82.3, AUC-96.6
ISIC 2019	C	2019	[33]	Mobile Net v2	BACC-81.2, AUC-97.1
ISIC 2019	C	2019	[33]	PNASNet	BACC-83.7, AUC-96.4
ISIC 2019	C	2019	[33]	ResNet50	BACC-82.0, AUC-97.8
ISIC 2019	C	2019	[33]	ResNet101	BACC-81.2, AUC-96.7
ISIC 2019	C	2019	[33]	ResNet152	BACC-81.8, AUC-96.9
ISIC 2019	C	2019	[33]	SENet	BACC-85.5, AUC-97.4
ISIC 2019	C	2019	[33]	VGG16	BACC-82.5, AUC-96.8
ISIC 2019	C	2019	[33]	VGG19	BACC-84.2, AUC-97.2
ISIC 2019	C	2019	[33]	Ensemble1(13 models)	BACC-88.3, AUC-98.8
ISIC 2019	C	2019	[33]	Ensemble2(best 3)	BACC-89.7, AUC-98.9
PH2	S	2017	[34]	FCN	DI-93.8
ISIC 2016	S	2017	[34]	FCN	ACC-95.3, DI-91.2, JA-84.7, SE-91.8, SP-96.6
ISBI 2017	S	2017	[34]	Convolution-	JA-78.4

Dataset	Task	Year	References	Model/architecture	Remarks
				Deconvolution Neural Network(CDNN)	
PH2	C	2018	[35]	AlexNet	ACC-98.61, SE-98.33, SP-98.93, P-97.73
PH2	S	2019	[36]	Encoder-Decoder Separable UNet	DI-86.93, JA-89.4, ACC-96.69, SE-96.51, SP-95.26
ISIC 2017	S	2019	[36]	Encoder-Decoder Separable UNet	DI-86.93, JA-79.26, ACC-94.31, SE-89.53, SP-96.32
ISIC 2016	S	2019	[36]	Encoder-Decoder Separable UNet	DI-93.03, JA-89.25, ACC-97.16, SE-94.7, SP-95.65
PH2	S/C	2020	[37]	AlexNet+VGG as feature extractor+ KNN classifier	SE-99.52, SP-99.62, AUC-99.9
National cancer center hospital, Tokyo	C	2020	[38]	FrCNN	Two class classification ACC-91.5, SE-93.3, SP-94.5
ISIC 2018	C	2020	[39]	MSM-CNN	BMCA-86.2, ACC-96.3, PR-91.3, AUC-98.1
Dermatological dataset	C	2017	[40]	Inception v3	ACC-72.1, AUC->91
Other datasets	C	2011	[41]	MLP	CR-86.73, SP-95.74, SE-78.43
Other datasets	C	2018	[42]	Pretrained AlexNet+SVM	ACC-94.2, SE-97.83, SP-90.75
Other datasets	S/C	2020	[43]	RCNN	SE-92.5, ACC-91.5
ISIC 2019	C	2020	[73]	Ensemble learning Fix-Efficient Net + metadata	AUC-95.4, SE-72.5

CHAPTER-4
PROPOSED WORK

At this point, we observed that convolutional neural network has been preferred over conventional handcraft-based CAD system for melanoma cancer detection and classification task. We introduced a more sophisticated and powerful framework for melanoma detection that involves concept of capsules along with convolution. Capsules Network has the ability to predict the presence of any object by encoding the spatial information. It uses the dynamic routing between capsules rather than max-pool layer, formerly used in deep neural networks. This work provides a robust, non-linear and equivariance model which provide better classification results.

This chapter will describe how capsule network is implemented on ISIC 2017 dataset. It starts with an overview of proposed framework, data visualization and data preprocessing. Finally, we move onto describing the overall architecture of proposed framework.

4.1 DATASETS

This section describes different benchmark datasets used for experiment analysis and comparing different methodologies proposed for segmentation and skin cancer classification. Moreover, this section provides information about sources and amount of training data and test data.

1) ISBI-ISIC Dataset

The ISIC dataset archive is used for training and validating the proposed model. It include ISIC 2016, 2017 and 2018 dataset contains 33,126 and 10,982 DICOM training and test images, respectively, with embedded metadata. These images were collected from 2000 patients, and each image has an associated patient id. This dataset was collaborated by International Skill Imaging Collaboration (ISIC). It is suitable for segmentation and classification tasks. The ISIC 2018 challenge dataset contains seven skin lesion types, namely malignant melanoma (MEL), benign keratosis (BKL), dermatofibroma (DF), melanocytic nevus (NV), basal cell carcinoma (BCC), actinic keratosis (AKIEC), and vascular lesion (VASC). Whereas the ISIC 2017 dataset consist of 2000 training images and datasets of 150

and 600 images for validation and testing, respectively belongs to three classes melanoma, seborrheic keratosis and benign nevi while the ISIC 2016 dataset has two classes melanoma and nevus.

2) PH2 dataset

The dataset consists of total of 200 dermoscopic images of a melanocytic lesion. The images are further classified into 80 images of common nevi, 80 images of atypical nevi, and 40 images of melanoma. The data was collaborated by the Dermatology Service of Hospital Pedro Hispano (Matosinhos, Portugal). The image has a size of 768×560 pixels. It found many applications related to segmentation and classification analysis.

Table 6 Distribution of ISBI 2017 dataset and PH2 dataset

Dataset	Training data				validation data				Test data			
	B	M	SK	Total	B	M	SK	Total	B	M	SK	Total
ISIC 2017	1372	374	254	2000	78	30	42	150	393	117	90	600
PH2	-	-	-	-	-	-	-	-	160	40	-	200

*B, M, and SK indicate benign nevi, melanoma, and seborrheic keratosis classes respectively

4.1.1 Exploratory Data analysis of ISIC dataset

The dataset consist of skin lesion images in DICOM, TFRecords and JPEG formats. Additionally, a text files train.csv, and test.csv containing metadata is also provided which include age, sex, lesion types and location of skin lesion in patients uniquely identified using patient id. The csv files can be read through pandas library while the DICOM images are read through pydicom library. DICOM files consist of images with header containg information about image. It is most commonly used format to store image samples in medical imaging. Moreover, the distribution of skin oesion among different occurring sites is shown in fig clearly indicates that occurance of 55% of skin lesion at torso and 20% at lower extremity.

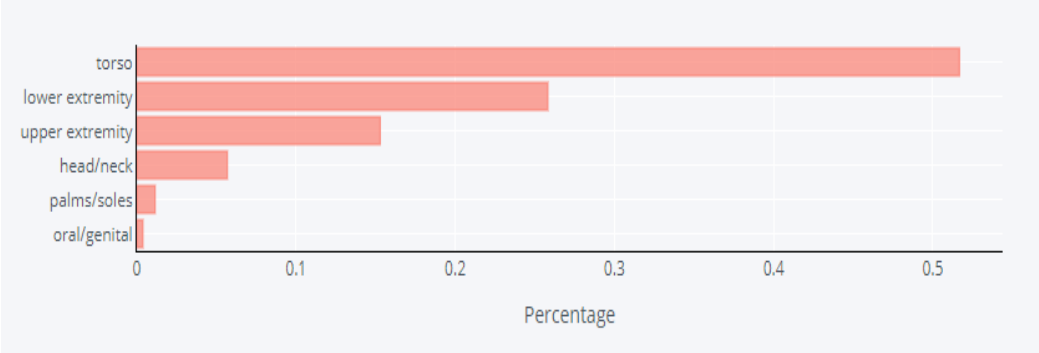

Fig. 20 Illustration of location of skin lesion diagnosed in patients

The probability distribution of benign and malignant tumor with respect to age is shown in figure 20 below . It clearly indicates that the patients having age 47-70 year are more risk of having malignant tumor or melanoma.

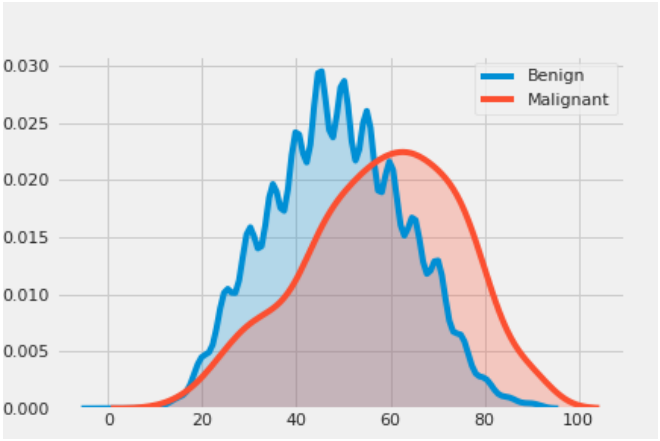

Fig. 21 Age distribution of benign and malignant skin cancer

Figure 21 shows the random images from the dataset, one may noticed that these images also contains hairs, bubbles and scale lines. These attributes acts as noise.

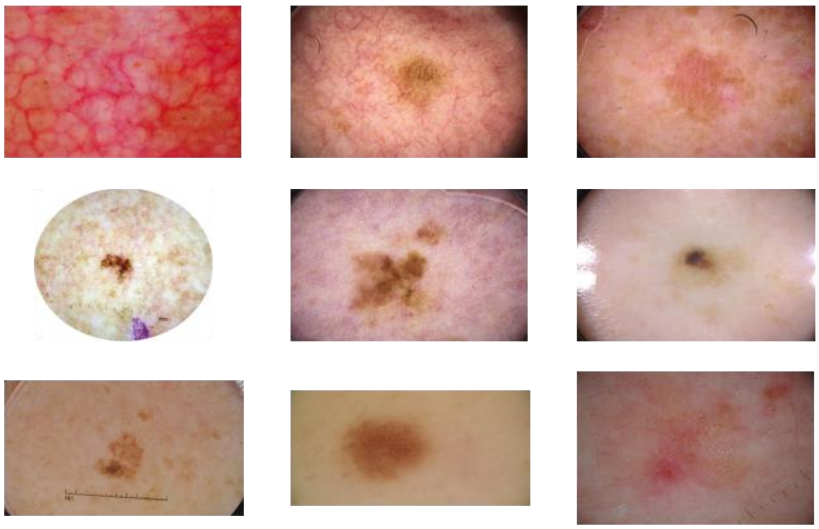

Fig. 22 Random samples of Training dataset

Histogram of skin lesion Images

Histogram is a graphical way of representing how frequently different pixels intensity occurs in a given image. It's range varies from 0 to 255. Study of histogram help to understand contrast, intensity variation and brightness of given image. Let's quickly dig into the histogram of benign and malignant skin lesion.

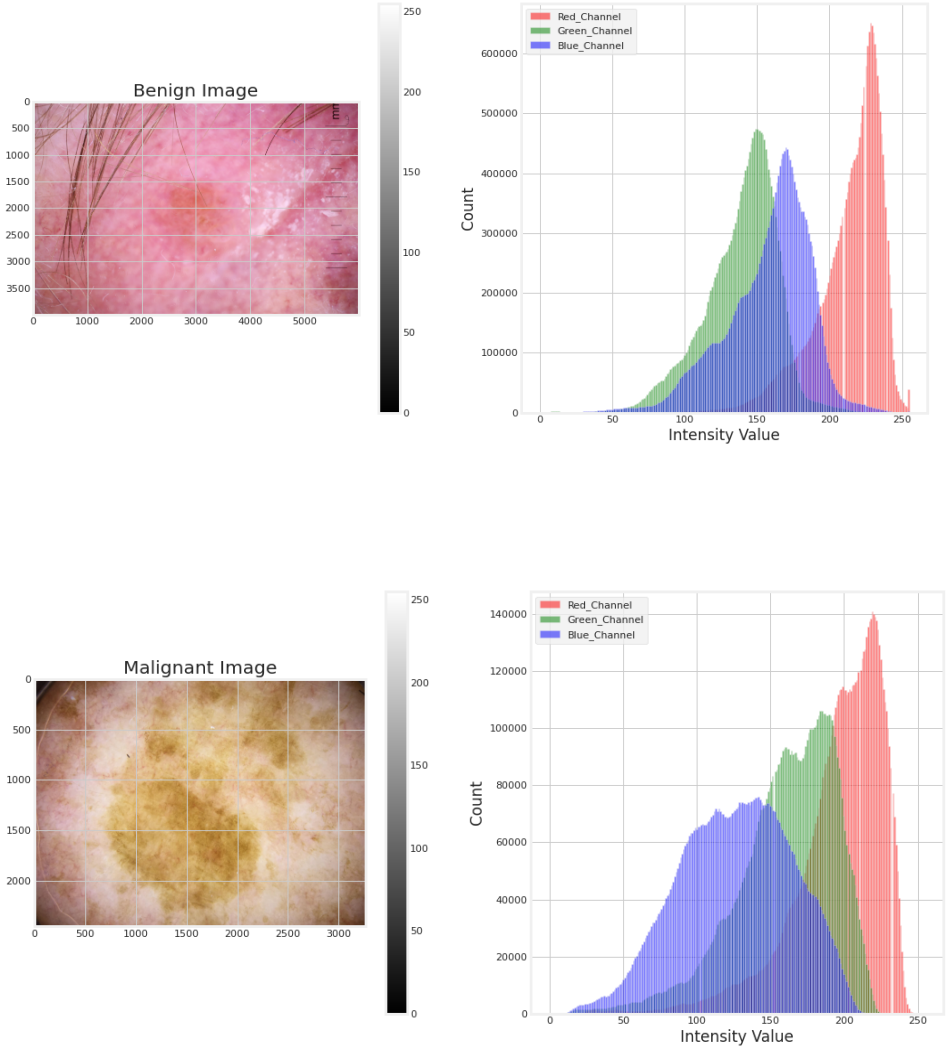

Fig. 23 Histogram of benign and malignant skin cancer

4.2 PROPOSED FRAMEWORK

The workflow of the proposed framework consists of four stages shown in figure 24. In the First stage, preprocessing is done and further generate masks from given annotated files. The next stage incorporates segmentation using Modified CapsNet, Finally, the classification is achieved using FixEfficientNet that predicts whether the given skin lesion image have melanoma or not. Moreover, the model perform class prediction of given PSL images.

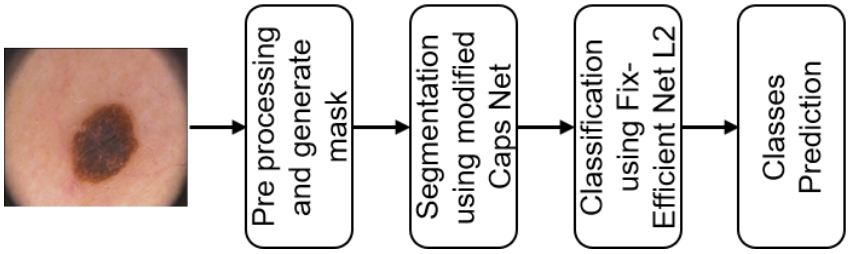

Fig. 24 Proposed Framework for Skin Cancer Detection and Classification

4.2.1 Data Preprocessing:

As discussed earlier, the ISIC 2017 dataset has images of different size so first step is resize all skin lesion images to 512×512 pixels grayscale image and histogram normalization is performed. Correspondingly their ground truth masks is also resized. Furthermore, data augmentation is used to generate more training samples which overcome the class imbalance problem and avoid overfitting. It is performed by processing random rotation, shearing and flipping of training images. The corresponding mask is also generated by applying equivalent transformation on ground truth mask given for the image(see fig 25).

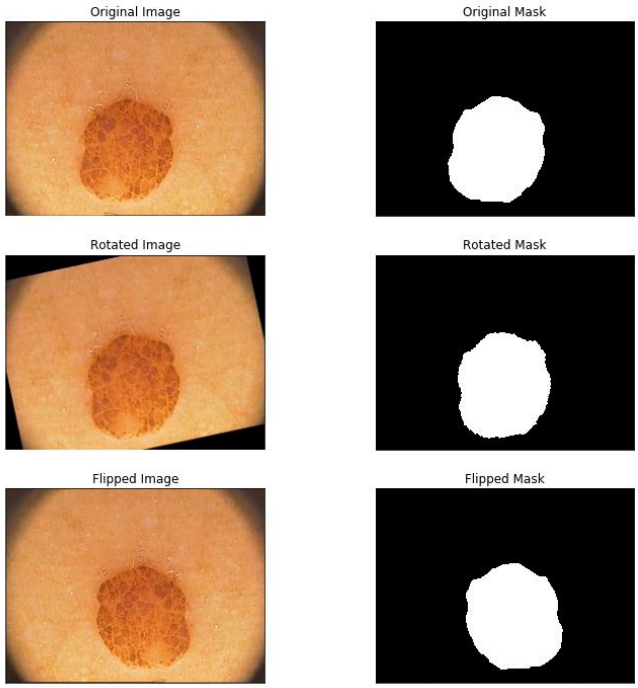

Fig. 25 Augmented Images and corresponding generated mask

4.2.2 Segmentation

At this point, all images are preprocessed and masks are generated which are fed to next stage. In this step, model instantiation is done and train the modified Caps Net model with the dice coefficient as a loss function.

$$DiceCoeff = \frac{2|G \cap S|}{|G| + |S|}$$

Where, G is the ground truth and S is segmented mask output. The proposed architecture as shown in Figure 26, consists of convolutional capsules, combined with UNet architecture. The skip connections are shown with dotted lines indicates features are copied from encoder part to decoder part so as to reimburse features loss during local routing.

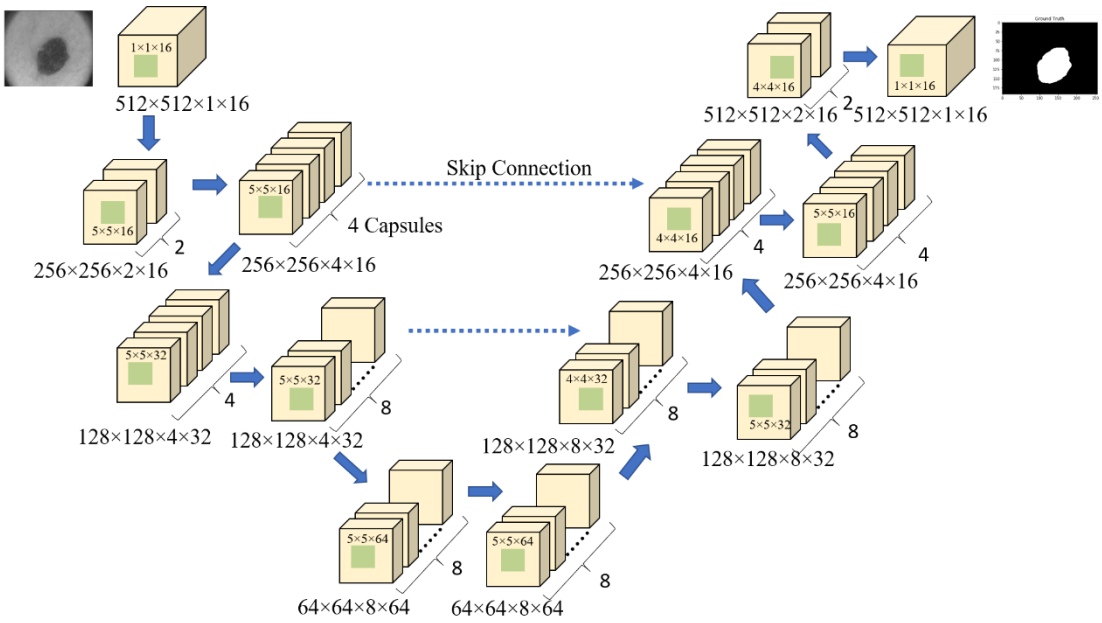

Fig. 26 Segmentation using Modified Capsule Network

In this modified CapsNet, the downsampling network consist of capsules. The network begins with a 2-D convolutional layer having 16 filters with size 5×5 and stride of 1, which outputs a 16 feature maps having same spatial dimension. Then, a second layer has two capsules consists of same filters size with stride 2 and outputs two 512×512×16 feature maps, similarly in every successive layers of encoder part the number of capsules doubles. In decoder part of architecture consist of deconvolutional layer along with the capsules which upsamples the capsules output by preceeding layers. Here, the utilization of routing by agreement is done at each primary capsule layers which help in reducing the trainable parameters.

4.2.3 Classification

The final Stage of our proposed architecture involve classification. We incorporate transfer learning approach for classification task. The Fix EfficientNet

pre-trained on ImageNet is used to classify skin lesion images with some minor modifications. The last layer of the model is replaced with a FC layer of size 128 neurons, followed by FC layer having three neurons corresponding to melanoma, nevus and seborrheic keratosis. Moreover, heavy data augmentation is done to avoid overfitting problem during training process. It consist of mobile inverted bottleneck layer(MBConv) and combines the advantages of both FixRes and Efficient Net. It improves the training method of EfficientNet by the" Fixing Resolution" fine-tuning process. Only a few top layers of Efficient Net architecture are modified which fixes the overfitting problem. The back-propagation is not performed on the whole network thus computationally cheap. FixEfficientNet has better top-1 and top-5 accuracy which shows state-of-the-art performance. The comparision of choosen model with other state-of -art model is shown below in figure 27.

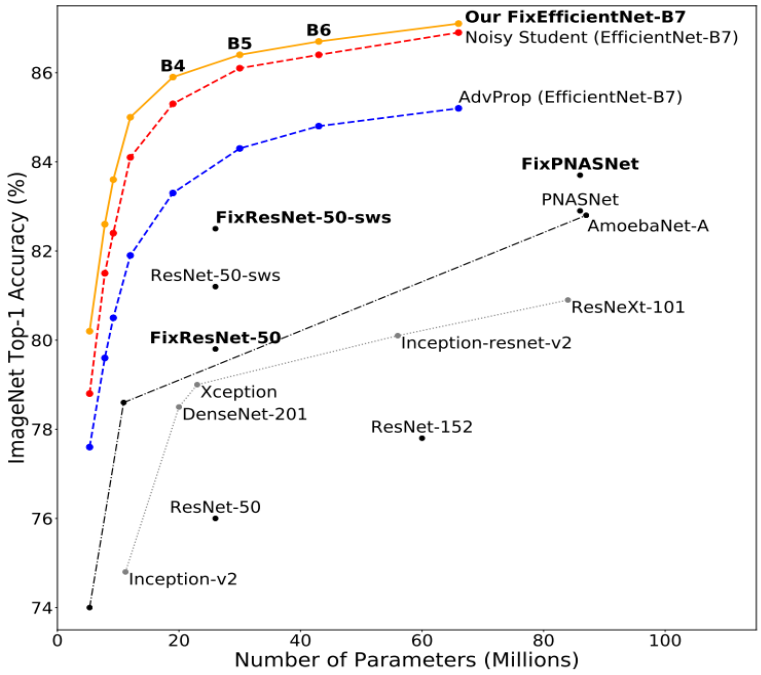

Fig. 27 Comparisison of Fix- Efficient Net with other state-of-the-art models in terms of number of parameters

CHAPTER-5

RESULTS AND DISCUSSION

Here, we discuss the tools, and technologies that we used to compile and validate our project and also illustrate the result. We also show the comparative analysis of our framework to others recently proposed architectures.

5.1 Tools and Packages

We use python programming language with anaconda platform. Following dependancies are required:

1. Python3.8
2. Anaconda3
3. Tensorflow
4. Keras
5. H5py
6. Pytorch
7. pydicom

All the codes are run on NVIDIA GPU: GTX 1050 and Quadro K420 with 16GB RAM.

5.2 METRICS

Mostly, the model performance of segmentation architecture was evaluated on Dice Coefficient/score, Free Response Receiver Operating Characteristic (FROC) and Accuracy achieved. But when we evaluate performance of proposed architecture for medical imaging then specificity and sensitivity are better measures to evaluate model performance than accuracy. However, the description of different metrics used to evaluate model are explained as follows:

1) Accuracy

Accuracy is the measure of correctly classify TP and TN out of total samples. The formula is as follows:

$$Accuracy = \frac{TP + TN}{TP + TN + FP + FN}$$

2) Dice Coefficient/Score

It is defined as the measure of overlap between predicted masks and ground truth mask. The formulae for calculating dice coefficient is as follows:

$$Dice\ Coefficient = \frac{2TP}{2TP + FN + FP}$$

3) Sensitivity

Sensitivity is the ability to identify the TP rate. The formula for sensitivity is given below:

$$Sensitivity = \frac{TP}{TP + FN}$$

4) **Specificity**

Specificity is defined as predicting a test negative when it is actually negative.

$$Specificity = \frac{TN}{FP + TN}$$

5.3 MODEL EVALUATION

5.3.1 Training

We train our model on ISIC 2017 dataset using the settings as follows: Stochastic gradient optimizer with decay0.9, momentum 0.9, initial learning rate 0.0001 and it increase by factor of 0.2 once validation loss plateau is reached. We also used data augmentation, 5×5 filter size and squash function in capsule layer. The model trains for 100 epochs. We implemented the network using torch, tensorflow and Keras library on Quadro K420 Nvidia GPU. The feature maps after first stage primary capsule layer is shown in figure below. It is clearly shown here that the feature vectors such as scaling, translation, localized skew, intensity variation etc are captured using capsules.

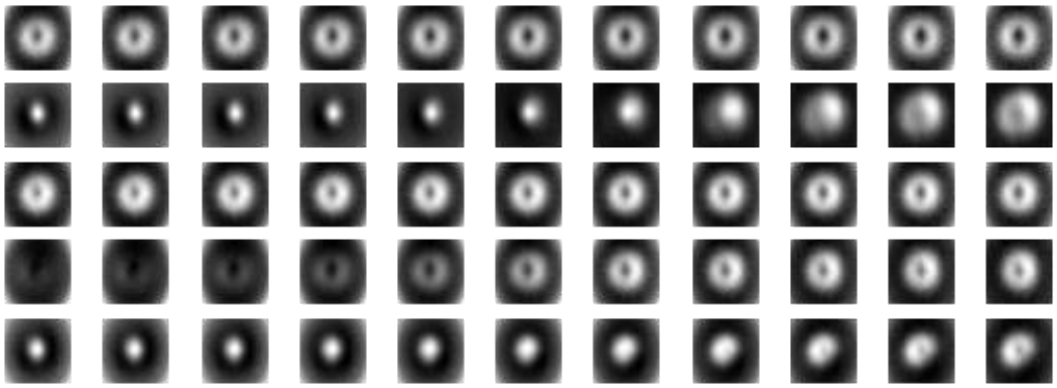

Fig. 28 Results of segmented Capsule Vectors.

The final segmentation results for melanoma, nevus and seborrheic keratosis are decribed in figure 27 below. The predicted result will undergo thresholding to generate binary mask.

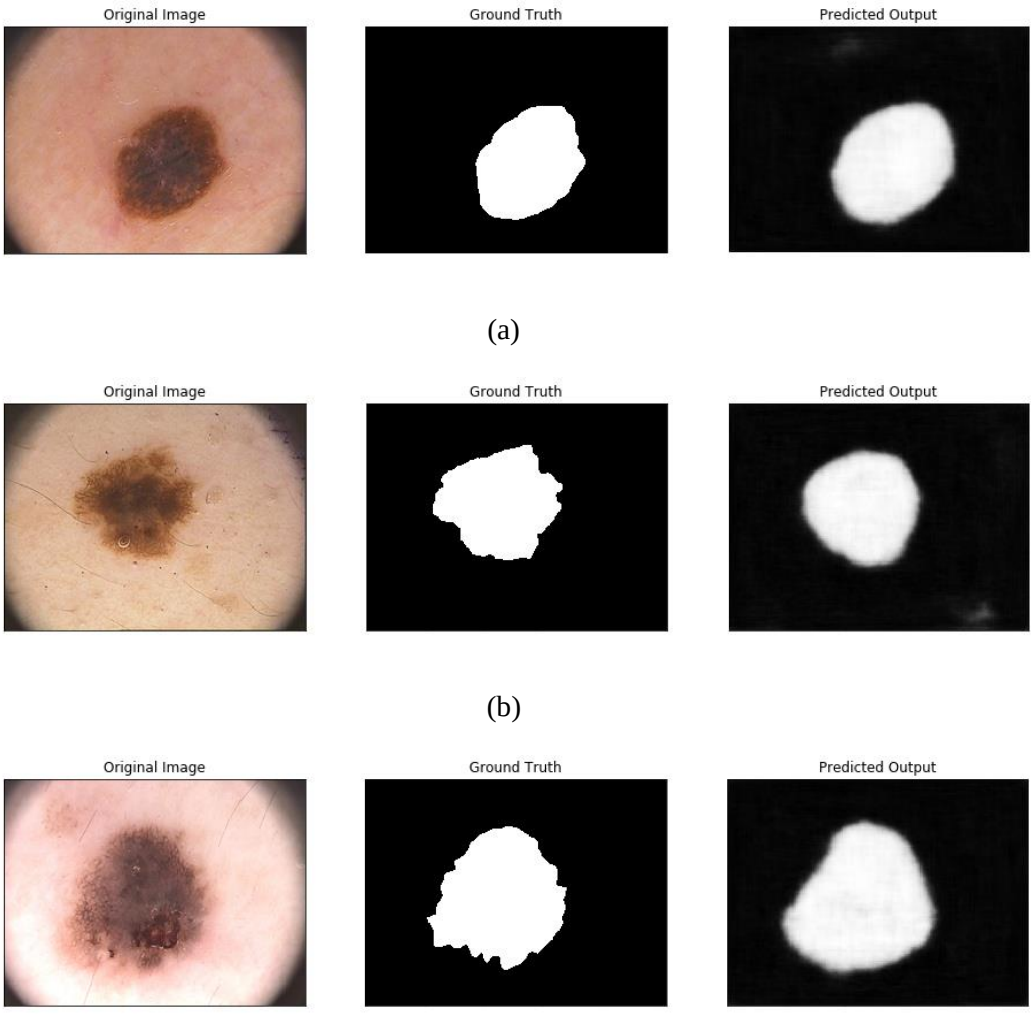

Fig. 29 Segmentation results of proposed architecture (a) benign (b) melanoma (c) seborrheic keratosis

To perform classification task, we employed fix-efficient net model. It is fed with the center cropped images of segmented skin lesion area and its classes. This model shows promisisng results on medical imaging analysissuch as lung nodule and breast tumor classification task. We choose this network as it incorporates compound scaling methods to achieve better accuracy results. The feature maps after first layer is shown below in figure 28.

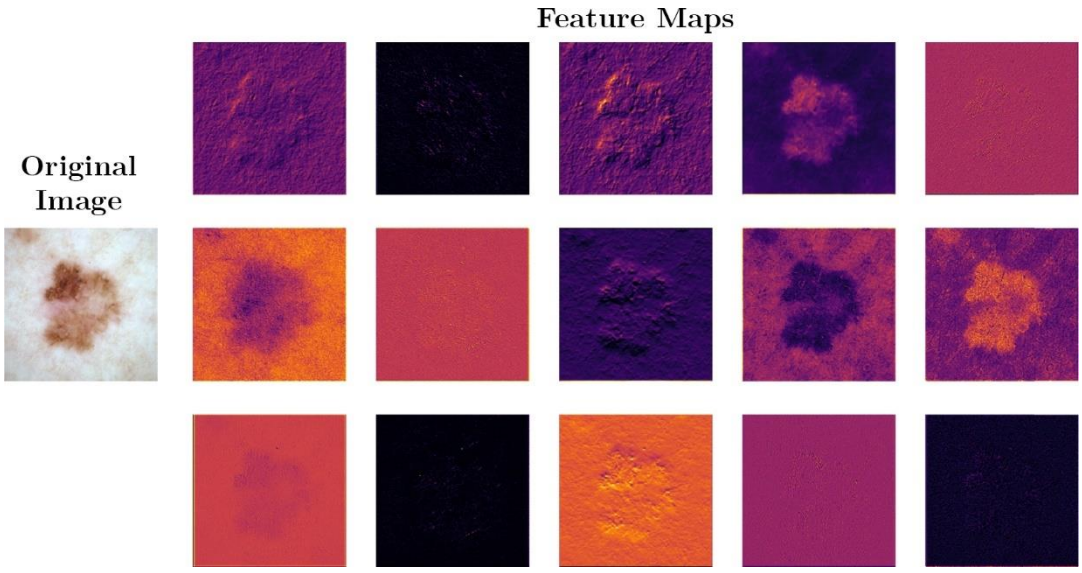

Fig. 30 Feature maps output after first layer processing by Fix EfficientNet

The major challenge in classifying skin lesion images are class imbalance and insufficient training samples. To overcome these challenges, we use transfer learning approach, moreover data augmentation like flipping, rotation etc. which increase the number of samples. Finally, parameters hypertuning is done by retraining the model by freezing upper layers and train lower layers to optimize the result. The overall performance of proposed architecture surpasses the results attained from previous models.

5.4 Model Analysis

1) Comparative Analysis of Segmentation Results

Table 7 shows the comparative analysis of segmentation results on the ISIC 2017 dataset, and Table 8 shows the comparative analysis of segmentation results on the PH2 dataset.

Table 7 Comparative Analysis of Segmentation results on ISIC 2017 dataset

Model	***ACC***	***SEN***	***SPEC***	***Dice Score***
FCN	84.6	74.8	94	80.2
DDN	95.9	95.1	95.9	93.1
U-Net	85.6	78.1	91.7	81.5
Modified CapsNet	**93.4**	**94.7**	**96.3**	**88.43**

Table 8 Comparative Analysis of Segmentation results on PH2 dataset

Model	*ACC*	*SEN*	*SPEC*	*Dice Score*
FCN	83.71	90.30	94.02	89.3
DDN	93.9	88.6	92.7	86.6
U-Net	92.55	81.63	97.61	82.78
Modified CapsNet	**93.43**	**86.63**	**96.61**	**89.36**

2) Comparative Analysis of Classification Results

The following table 9 shows the comparative analysis of the proposed architecture with state-of-the-art techniques, which suggests that our model outperforms other methods. And figure 10 shows the plot training and validation accuracy and loss of proposed method.

Table 9 Comparative Analysis of Classification result with different state-of-art methods.

Model	*Accuracy (%)*
ResNet	82.1
EnsembleResNet	88.4
MobileNet	81.2
FixEfficientNet	**98.03**

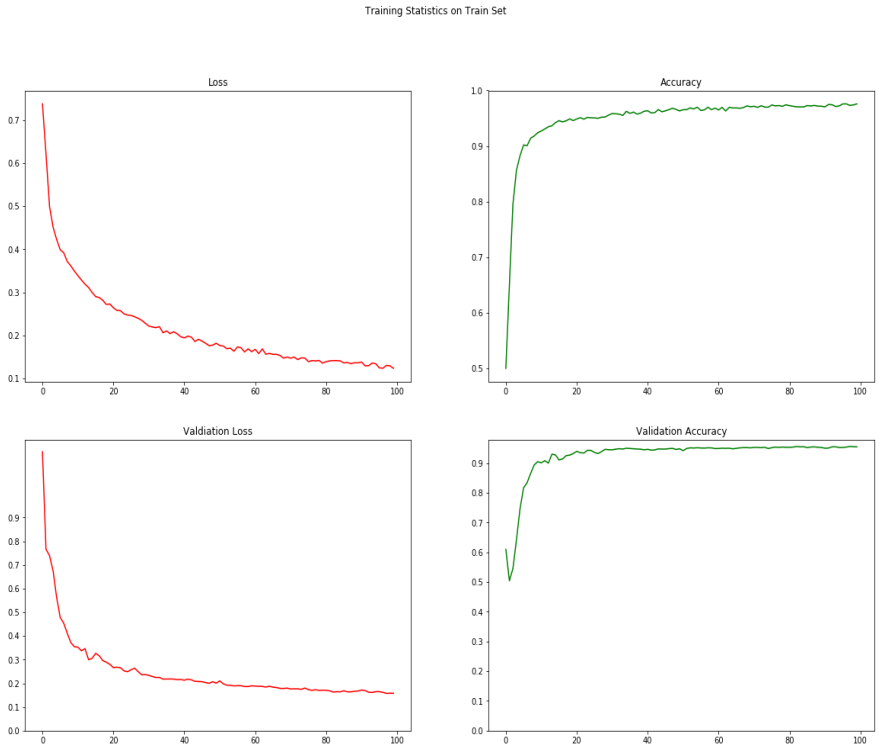

Fig. 31 Performance Analysis of Proposed Network.

3) Analysis of Hyper-parameters

The following table 8 shows the numbers of hyper-parameters required to tune while detecting and classifying skin lesion images.

Table 10 Analysis of Hyper-parameters

Phase	***Number of Parameters***
Detection	1.4M
Classification	66M

CHAPTER-6

CONCLUSION AND FUTURE WORK

6.1 CONCLUSION

Diagnosing melanoma at an early stage reduces the mortality rate. We discussed the fundamentals of the CAD system and reviewed the recently proposed design to diagnose skin lesion images. This work provides a detailed survey of all stages employed in the CAD system. According to the review of classical methods, SVM and ANN are frequently used classifiers to classify lesion images. The relevant feature extraction and selection procedure is key to a successful classification model. Thus, in the literature survey, we reviewed some famous research on feature extraction and feature selection techniques and concluded that GLCM and ABCD parameters are primarily used for skin lesion classification. A comprehensive study of recent CNN and deep learning-based research for the segmentation and classification tasks. It was the objective of this work to develop a more robust and efficient computer-assisted skin lesion diagnostic system and classify melanoma cancer. This type of system will help dermatologists to diagnose more precisely and plan the treatment procedure.

Our proposed framework uses the concept of Capsules embedded into UNet architecture to segment skin lesions, and applied pre-trained fix-EfficientNet to classify melanoma skin cancer. The model has less parameters to train while comparing to other models. The models is trained and validate on datasets: ISIC 2017 and PH2 publically available. The most stringent requirement of any diagnostics system is less number of parameters which affects storage requirements and computational complexity. Our proposed architecture has a relatively low trainable parameters with around 1.4 M at the segmentation stage. Moreover, the dice score of 88.43 suggests that modes generate masks with higher accuracy and precision to ground truth masks using a modified capsule network. Finally, the classification into melanoma, seborrheic kurtosis, nevus and non-melanoma skin cancer is done by transfer learning approach. A pre-trained FixEfficientNet model, already trained on IMAGENET is chosen to perform multi-class classification. The model achieved an 88.3% dice score, 93.4% accuracy, 94.7 % sensitivity, and

96.3% of specificity. The performance achieved outperforms conventional state-of-art-methods.

6.2 FUTURE WORK

The skin lesion images from different sources have different color variations and contain hairs and air bubbles which poses a challenge to accurate classification. However, many methods employ preprocessing techniques to overcome this challenge which generally blurs the image. Sometimes, images contain irregular boundaries, making it complex to segment an image and produce false results. Low contrast images and resizing of lesion images during preprocessing also affect the segmentation result and loss of many features. Some of the available public datasets have a class imbalance problem which required attention as many classifiers have had poor classification performance to classes having fewer samples.

These are many improvements that can be used to enhance the segmentation and classification tasks in the future. First, researchers can combine metadata or histopathological data of patients with other features to increase the accuracy. Second, there is much less research work done on the evolution of skin lesions, so researchers can propose a method to analyze the spread and growth of skin lesions. Finally, attention is required to study microscopic images and molecular-level analysis of skin lesions to provide an accurate and effective skin cancer diagnosis.

REFERENCES

[1] H. Sung, J. Ferlay, R. L. Siegel, M. Laversanne, I. Soerjomataram, A. Jemal, and F. Bray, "Global cancer statistics 2020: GLOBOCAN estimates of incidence and mortality worldwide for 36 cancers in 185 countries.," *CA. Cancer J. Clin.*, Feb. 2021.

[2] B. Lindelof and M. A. Hedblad, "Accuracy in the clinical diagnosis and pattern of malignant melanoma at a dermatological clinic," *J. Dermatol.*, vol. 21, no. 7, pp. 461–464, 1994.

[3] G. Argenziano and P. Soyer, "Dermoscopy of pigmented skin lesions – a valuable tool for early," *Lancet Oncol.*, vol. 2, pp. 443–449, Aug. 2001.

[4] G. A. Eddine, "Skin Lesion Classification Using Deep Neural Network," *arXiv*, no. 8, 2019.

[5] G. Argenziano and H. P. Soyer, "Dermoscopy of pigmented skin lesions – a valuable tool for early," *Lancet Oncol.*, vol. 2, no. 7, pp. 443–449, 2001.

[6] A. Lorber, M. Wiltgen, R. Hofmann-Wellenhof, S. Koller, W. Weger, V. Ahlgrimm-Siess, J. Smolle, and A. Gerger, "Correlation of image analysis features and visual morphology in melanocytic skin tumours using in vivo confocal laser scanning microscopy," *Skin Res. Technol.*, vol. 15, pp. 237–241, Jun. 2009.

[7] R. Hofmann-Wellenhof, E. Wurm, V. Ahlgrimm-Siess, E. Richtig, S. Koller, J. Smolle, and A. Gerger, "Reflectance Confocal Microscopy-State-of-Art and Research Overview," *Semin. Cutan. Med. Surg.*, vol. 28, pp. 172–179, Sep. 2009.

[8] L. Serrone, F. Solivetti, M. Thorel, L. Eibenschutz, P. Donati, and C. Catricalà, "High frequency ultrasound in the preoperative staging of primary melanoma: A statistical analysis," *Melanoma Res.*, vol. 12, pp. 287–290, Jun. 2002.

[9] A. Blum, M. Schmid-Wendtner, V. Mauss-Kiefer, J. Eberle, C. Kuchelmeister, and D. Dill-Müller, "Ultrasound Mapping of Lymph Node and Subcutaneous Metastases in Patients with Cutaneous Melanoma: Results of a Prospective Multicenter Study," *Dermatology*, vol. 212, pp. 47–52, Jan. 2006.

[10] J. Mäurer, F. Knollmann, D. SCHLUMS, C. Garbe, T. Vogl, J. BIER, and R. Felix, "Role of High-Resolution Magnetic Resonance Imaging for Differentiating Melanin-Containing Skin Tumors," *Invest. Radiol.*, vol. 30, pp. 638–643, Dec. 1995.

We[11] I. Ono and F. Kaneko, "Magnetic resonance imaging for diagnosing skin tumors," *Clin. Dermatol.*, vol. 13, pp. 393–399, Jul. 1995.

[12] J. Welzel, "Optical coherence tomography in dermatology: a review.," *Ski. Res. Technol. Off. J. Int. Soc. Bioeng. Ski. [and] Int. Soc. Digit. Imaging Ski. [and] Int. Soc. Ski. Imaging*, vol. 7, no. 1, pp. 1–9, Feb. 2001.

[13] M. Carrara, A. Bono, C. Bartoli, A. Colombo, M. Lualdi, D. Moglia, N. Santoro, T. Elena, S. Tomatis, G. Tragni, M. Santinami, and R. Marchesini, "Multispectral imaging and artificial neural network: Mimicking the management decision of the clinician facing pigmented skin lesions," *Phys. Med. Biol.*, vol. 52, pp. 2599–2613, Jun. 2007.

[14] M. Carrara, S. Tomatis, A. Bono, C. Bartoli, D. Moglia, M. Lualdi, A. Colombo, M. Santinami, and R. Marchesini, "Automated segmentation of pigmented skin lesions in multispectral imaging," *Phys. Med. Biol.*, vol. 50, pp. N345-57, Dec. 2005.

[15] D. A. Shoieb, S. M. Youssef, and W. M. Aly, "Computer-Aided Model for Skin Diagnosis Using Deep Learning," *J. Image Graph.*, vol. 4, no. 2, pp. 122–129, 2016.

[16] M. E. Celebi, H. A. Kingravi, H. Iyatomi, J. Lee, Y. A. Aslandogan, W. Van Stoecker, R. Moss, J. M. Malters, and A. A. Marghoob, "Fast and accurate border detection in dermoscopy images using statistical region merging," in *Proc.SPIE*, 2007, vol. 6512.

[17] I. Maglogiannis and C. N. Doukas, "Overview of advanced computer vision systems for skin lesions characterization," *IEEE Trans. Inf. Technol. Biomed.*, vol. 13, no. 5, pp. 721–733, 2009.

[18] M. Silveira and J. S. Marques, "Level set segmentation of dermoscopy images," in *2008 5th IEEE International Symposium on Biomedical Imaging: From Nano to Macro*, 2008, pp. 173–176.

[19] B. Erkol, R. Moss, R. Stanley, W. Stoecker, and E. Hvatum, "Automatic lesion boundary detection in dermoscopy images using gradient vector flow snakes," *Skin Res. Technol.*, vol. 11, pp. 17–26, Mar. 2005.

[20] J. A. Jaleel, S. Salim, and R. B. Aswin, "Computer aided detection of skin cancer," *Proc. IEEE Int. Conf. Circuit, Power Comput. Technol. ICCPCT 2013*, pp. 1137–1142, 2013.

[21] Q. Abbas, I. Fondón, and M. Rashid, "Unsupervised skin lesions border detection via two-dimensional image analysis," *Comput. Methods Programs Biomed.*, vol. 104, no. 3, pp. e1–e15, 2011.

[22] M. G. Fleming, C. Steger, J. Zhang, J. Gao, A. B. Cognetta, L. Pollak, and C. R. Dyer, "Techniques for a structural analysis of dermatoscopic imagery," *Comput. Med. Imaging Graph.*, vol. 22, no. 5, pp. 375–389, 1998.

[23] Q. Li, L. Zhang, J. You, D. Zhang, and P. Bhattacharya, "Dark line detection with line width extraction," in *2008 15th IEEE International Conference on Image Processing*, 2008, pp. 621–624.

[24] V. Srividhya, K. Sujatha, R. S. Ponmagal, G. Durgadevi, L. Madheshwaran, and V., "Vision based Detection and Categorization of Skin lesions using Deep Learning Neural networks," *Procedia Comput. Sci.*, vol. 171, pp. 1726–1735, 2020.

[25] M. M. Rahman, P. Bhattacharya, and B. C. Desai, "A multiple expert-based melanoma recognition system for dermoscopic images of pigmented skin lesions," pp. 1–6, 2008.

[26] M. Krishna Monika, N. Arun Vignesh, C. Usha Kumari, M. N. V. S. S. Kumar, and E. Laxmi Lydia, "Skin cancer detection and classification using machine learning," *Mater. Today Proc.*, vol. 33, no. xxxx, pp. 4266–4270, 2020.

[27] C. Dolianitis, J. Kelly, R. Wolfe, and P. Simpson, "Comparative Performance of 4 Dermoscopic Algorithms by Nonexperts for the Diagnosis of Melanocytic Lesions," *Arch. Dermatol.*, vol. 141, no. 8, pp. 1008–1014, Aug. 2005.

[28] R. Braun, L. Thomas, S. Dusza, O. Gaide, S. Menzies, A. Blum, G. Argenziano, I. Zalaudek, A. Kopf, H. Rabinovitz, M. Oliviero, A. Perrinaud, H. Cabo, M. Pizzichetta, L. Pozo, D. Langford, M. Tanaka, T. Saida, A. Perusquía-Ortiz, and A. A. Marghoob, "Dermoscopy of Acral Melanoma: A Multicenter Study on Behalf of the International Dermoscopy Society," *Dermatology*, vol. 227, Nov. 2013.

[29] M. Keefe, D. Dick, and A. Wakeel, "A study of the value of the seven-point checklist in distinguish benign pigmented lesions from melanoma," *Clin. Exp. Dermatol.*, vol. 15, pp. 167–171, Jun. 1990.

[30] O. Abuzaghleh, B. D. Barkana, and M. Faezipour, "Noninvasive real-time automated skin lesion analysis system for melanoma early detection and prevention," *IEEE J. Transl. Eng. Heal. Med.*, vol. 3, no. March, 2015.

[31] Y. Saeys, I. Inza, and P. Larrañaga, "A review of feature selection techniques in bioinformatics," *Bioinformatics*, vol. 23, no. 19, pp. 2507–2517, Oct. 2007.

[32] G. Chandrashekar and F. Sahin, "A survey on feature selection methods," *Comput. Electr. Eng.*, vol. 40, no. 1, pp. 16–28, 2014.

[33] S. Khalid, T. Khalil, and S. Nasreen, "A survey of feature selection and feature extraction techniques in machine learning," in *2014 Science and Information Conference*, 2014, pp. 372–378.

[34] S. Dreiseitl, L. Ohno-Machado, H. Kittler, S. Vinterbo, H. Billhardt, and M. Binder, "A comparison of machine learning methods for the diagnosis of pigmented skin lesions," *J. Biomed. Inform.*, vol. 34, no. 1, pp. 28–36, 2001.

[35] K. Ramlakhan and Y. Shang, "A mobile automated skin lesion classification system," *Proc. - Int. Conf. Tools with Artif. Intell. ICTAI*, pp. 138–141, 2011.

[36] M. Burroni, R. Corona, G. Dell'Eva, F. Sera, R. Bono, P. Puddu, R. Perotti, F. Nobile, L. Andreassi, and P. Rubegni, "Melanoma Computer-Aided Diagnosis Reliability and Feasibility Study," *Clin. Cancer Res.*, vol. 10, pp. 1881–1886, Apr. 2004.

[37] M. E. Celebi, H. Iyatomi, W. V. Stoecker, R. H. Moss, H. S. Rabinovitz, G. Argenziano, and H. P. Soyer, "Automatic detection of blue-white veil and related structures in dermoscopy images," *Comput. Med. Imaging Graph.*, vol. 32, no. 8, pp. 670–677, 2008.

[38] S. V. Patwardhan, S. Dai, and A. P. Dhawan, "Multispectral image analysis and classification of melanoma using fuzzy membership based partitions," *Comput. Med. Imaging Graph.*, vol. 29, no. 4, pp. 287–296, 2005.

[39] S. V. Patwardhan, A. P. Dhawan, and P. A. Relue, "Classification of melanoma using tree structured wavelet transforms," *Comput. Methods Programs Biomed.*, vol. 72, no. 3, pp. 223–239, 2003.

[40] M. Burroni, P. Sbano, G. Cevenini, M. Risulo, G. Dell'eva, P. Barbini, C. Miracco, M. Fimiani, L. Andreassi, and P. Rubegni, "Dysplastic naevus vs. in situ melanoma: Digital dermoscopy analysis," *Br. J. Dermatol.*, vol. 152, pp. 679–684, May 2005.

[41] S. Gilmore, R. Hofmann-Wellenhof, and P. Soyer, "A support vector machine for decision support in melanoma recognition," *Exp. Dermatol.*, vol. 19, pp. 830–835, Sep. 2010.

[42] X. Yuan, Z. Yang, G. Zouridakis, and N. Mullani, "SVM-based Texture Classification and Application to Early Melanoma Detection," in *2006 International Conference of the IEEE Engineering in Medicine and Biology Society*, 2006, pp. 4775–4778.

[43] Y. Yuan, "Automatic skin lesion segmentation with fully convolutional-deconvolutional networks," *arXiv*, pp. 2–5, 2017.

[44] M. H. Jafari, N. Karimi, E. Nasr-Esfahani, S. Samavi, S. M. R. Soroushmehr, K. Ward, and K. Najarian, "Skin lesion segmentation in clinical images using deep learning," in *2016 23rd International Conference on Pattern Recognition (ICPR)*, 2016, pp. 337–342.

[45] M. A. Al-masni, M. A. Al-antari, M. T. Choi, S. M. Han, and T. S. Kim, "Skin lesion segmentation in dermoscopy images via deep full resolution convolutional networks," *Comput. Methods Programs Biomed.*, vol. 162, pp. 221–231, 2018.

[46] H. Li, X. He, F. Zhou, Z. Yu, D. Ni, S. Chen, T. Wang, and B. Lei, "Dense Deconvolutional Network for Skin Lesion Segmentation," *IEEE J. Biomed. Heal. Informatics*, vol. 23, no. 2, pp. 527–537, 2019.

[47] Y. Tang, F. Yang, S. Yuan, and C. Zhan, "A multi-stage framework with context information fusion structure for skin lesion segmentation," *arXiv*, no. Isbi, pp. 2019–2022, 2018.

[48] B. Lei, Z. Xia, F. Jiang, X. Jiang, Z. Ge, Y. Xu, J. Qin, S. Chen, T. Wang, and S. Wang, "Skin lesion segmentation via generative adversarial networks with dual discriminators," *Med. Image Anal.*, vol. 64, p. 101716, Aug. 2020.

[49] N. Navab, J. Hornegger, W. M. Wells, and A. F. Frangi, "Medical Image Computing and Computer-Assisted Intervention - MICCAI 2015: 18th International Conference Munich, Germany, October 5-9, 2015 proceedings, part III," *Lect. Notes Comput. Sci. (including Subser. Lect. Notes Artif. Intell. Lect. Notes Bioinformatics)*, vol. 9351, no. Cvd, pp. 12–20, 2015.

[50] Z. Mirikharaji and G. Hamarneh, "Star Shape Prior in Fully Convolutional Networks for Skin Lesion Segmentation," *Lect. Notes Comput. Sci. (including Subser. Lect. Notes Artif. Intell. Lect. Notes Bioinformatics)*, vol. 11073 LNCS, pp. 737–745, 2018.

[51] J. Long, E. Shelhamer, and T. Darrell, "Imperforated Anus in Calves and its Surgical Treatment," *Intas Polivet*, vol. 10, no. 2, pp. 227–228, 2009.

[52] Y. Song, E. L. Tan, X. Jiang, J. Z. Cheng, D. Ni, S. Chen, B. Lei, and T. Wang, "Accurate cervical cell segmentation from overlapping clumps in pap smear images," *IEEE Trans. Med. Imaging*, vol. 36, no. 1, pp. 288–300, 2017.

[53] M. S. Elmahdy, S. S. Abdeldayem, and I. A. Yassine, "Low quality dermal image classification using transfer learning," in *2017 IEEE EMBS*

International Conference on Biomedical & Health Informatics (BHI), 2017, pp. 373–376.

[54] A. R. Lopez, X. Giro-i-Nieto, J. Burdick, and O. Marques, "Skin lesion classification from dermoscopic images using deep learning techniques," in *2017 13th IASTED International Conference on Biomedical Engineering (BioMed)*, 2017, pp. 49–54.

[55] J. Yap, W. Yolland, and P. Tschandl, "Multimodal skin lesion classification using deep learning," *Exp. Dermatol.*, vol. 27, no. 11, pp. 1261–1267, 2018.

[56] A. Singhal, R. Shukla, P. K. Kankar, S. Dubey, S. Singh, and R. B. Pachori, "Comparing the capabilities of transfer learning models to detect skin lesion in humans," *Proc. Inst. Mech. Eng. Part H J. Eng. Med.*, vol. 234, no. 10, pp. 1083–1093, 2020.

[57] A. Mahbod, G. Schaefer, C. Wang, G. Dorffner, R. Ecker, and I. Ellinger, "Transfer learning using a multi-scale and multi-network ensemble for skin lesion classification," *Comput. Methods Programs Biomed.*, vol. 193, p. 105475, 2020.

[58] M. A. Kadampur and S. Al Riyaee, "Skin cancer detection: Applying a deep learning based model driven architecture in the cloud for classifying dermal cell images," *Informatics Med. Unlocked*, vol. 18, p. 100282, 2020.

[59] P. Yao, S. Shen, M. Xu, P. Liu, F. Zhang, J. Xing, P. Shao, B. Kaffenberger, and R. X. Xu, "Single Model Deep Learning on Imbalanced Small Datasets for Skin Lesion Classification," vol. 10000, pp. 1–10, 2021.

[60] A. Mahbod, G. Schaefer, C. Wang, R. Ecker, and I. Ellinge, "Skin Lesion Classification Using Hybrid Deep Neural Networks," *ICASSP, IEEE Int. Conf. Acoust. Speech Signal Process. - Proc.*, vol. 2019-May, pp. 1229–1233, 2019.

[61] D. de A. Rodrigues, R. F. Ivo, S. C. Satapathy, S. Wang, J. Hemanth, and P. P. R. Filho, "A new approach for classification skin lesion based on transfer learning, deep learning, and IoT system," *Pattern Recognit. Lett.*, vol. 136, pp. 8–15, 2020.

[62] A. G. C. Pacheco, A. R. Ali, and T. Trappenberg, "Skin cancer detection based on deep learning and entropy to detect outlier samples," *arXiv*, pp. 1–6, 2019.

[63] Y. Yuan, M. Chao, and Y. C. Lo, "Automatic Skin Lesion Segmentation Using Deep Fully Convolutional Networks with Jaccard Distance," *IEEE Trans. Med. Imaging*, vol. 36, no. 9, pp. 1876–1886, 2017.

[64] K. M. Hosny, M. A. Kassem, and M. M. Foaud, "Skin Cancer Classification using Deep Learning and Transfer Learning," in *2018 9th Cairo International Biomedical Engineering Conference (CIBEC)*, 2018, pp. 90–93.

[65] P. Tang, Q. Liang, X. Yan, S. Xiang, W. Sun, D. Zhang, and G. Coppola, "Efficient skin lesion segmentation using separable-Unet with stochastic weight averaging," *Comput. Methods Programs Biomed.*, vol. 178, pp. 289–301, Sep. 2019.

[66] J. Amin, A. Sharif, N. Gul, M. A. Anjum, M. W. Nisar, F. Azam, and S. A. C. Bukhari, "Integrated design of deep features fusion for localization and classification of skin cancer," *Pattern Recognit. Lett.*, vol. 131, pp. 63–70, 2020.

[67] S. Jinnai, N. Yamazaki, Y. Hirano, Y. Sugawara, Y. Ohe, and R. Hamamoto, "The Development of a Skin Cancer Classification System for Pigmented Skin Lesions Using Deep Learning," *Biomolecules*, vol. 10, no. 8. 2020.

[68] A. Mahbod, G. Schaefer, C. Wang, G. Dorffner, R. Ecker, and I. Ellinger, "Transfer learning using a multi-scale and multi-network ensemble for skin lesion classification," *Comput. Methods Programs Biomed.*, vol. 193, p. 105475, Sep. 2020.

[69] A. Esteva, B. Kuprel, R. A. Novoa, J. Ko, S. M. Swetter, H. M. Blau, and S. Thrun, "Dermatologist-level classification of skin cancer with deep neural networks," *Nature*, vol. 542, no. 7639, pp. 115–118, 2017.

[70] D. Ruiz, V. Berenguer, A. Soriano, and B. Sánchez, "A decision support system for the diagnosis of melanoma: A comparative approach," *Expert Syst. Appl.*, vol. 38, no. 12, pp. 15217–15223, 2011.

[71] U.-O. Dorj, K.-K. Lee, J.-Y. Choi, and M. Lee, "The skin cancer classification using deep convolutional neural network," *Multimed. Tools Appl.*, vol. 77, no. 8, pp. 9909–9924, 2018.

[72] S. S. Han, I. J. Moon, W. Lim, I. S. Suh, S. Y. Lee, J. I. Na, S. H. Kim, and S. E. Chang, "Keratinocytic Skin Cancer Detection on the Face Using Region-Based Convolutional Neural Network," *JAMA Dermatology*, vol. 156, no. 1, pp. 29–37, 2020.

[73] N. Gessert, M. Nielsen, M. Shaikh, R. Werner, and A. Schlaefer, “Skin lesion classification using ensembles of multi-resolution EfficientNets with meta data,” MethodsX, vol. 7, p. 100864, 2020.